\$ SUPER

Contents lists available at ScienceDirect

Materials Today Advances

journal homepage: www.journals.elsevier.com/materials-today-advances/



Characterization of plasma discharge tube for cancer treatment

Vikas Soni ^{a,*} ^o, Li Lin ^{a,1}, Anmol Taploo ^{a,1}, Jonathan H. Sherman ^b, Michael Keidar ^{a,**}

- ^a Micro Propulsion and Nanotechnology Lab (MPNL), Department of Mechanical and Aerospace Engineering, School of Engineering and Applied Science, The George Washington University, 800 22nd St NW, Suite 3000, Washington, DC, 20052, USA
- b Department of Newrosurgery, Rutgers Robert Wood Johnson Medical School, Rutgers Cancer Institute of New Jersey, 10 Plum Street, 9th Floor, New Brunswick, NJ, 08901, USA

ARTICLE INFO

Keywords: Plasma discharge tube (PDT) Cold plasma tube (CPT) Electromagnetic field (EMF) Tumor treating fields (TTF) Cold atmospheric plasma (CAP) Non-thermal plasma Cold plasma Glow discharge Ionization Electric field Magnetic field Optical emission spectroscopy (OES) Rayleigh microwave scattering Reactive oxygen species Reactive nitrogen species Cancer therapy Sensitization Plasma medicine Glioblastoma

ABSTRACT

In this study, we propose a novel approach utilizing a Plasma Discharge Tube (PDT) system for cancer therapy. The PDT operates as a closed, non-invasive plasma delivery platform capable of generating a spectrum of reactive oxygen and nitrogen species (RONS) and electromagnetic (EM) fields that can influence cancer cell behavior. To fully understand its therapeutic potential, we conducted a comprehensive physical and biological characterization using Optical Emission Spectroscopy (OES) to identify active plasma species, EM wave emission measurements to quantify field intensity, Rayleigh Microwave Scattering (RMS) to estimate electron density, EM sensors and near-field probe mapping to evaluate field distribution, and Intensified Charge-Coupled Device (ICCD) imaging to visualize plasma morphology and propagation. Initial in vitro studies demonstrated potent cytotoxic effects of PDT on glioblastoma (GBM) cell lines, including A172, T98G, and U87MG. Furthermore, when combined with chemotherapeutic agents such as Elesclomol (STA-4783), Paclitaxel (Taxol), and Temocolomide (TMZ), PDT pretreatment enhanced drug sensitivity and reduced cell viability more effectively than either treatment alone. Overall, these findings suggest that the PDT system can modulate tumor cell response both as a standalone modality and in combination with drugs through plasma-induced biochemical and biophysical mechanisms, providing a promising new strategy for overcoming therapeutic resistance, advancing personalized cancer treatment and improving patient outcomes.

1. Introduction

Synergism

Cold plasma is an ionized gas generated at room temperature and under atmospheric pressure conditions that contains electrons, ions, neutral particles, ultraviolet (UV) emission, and electromagnetic (EM) effect. [1–4]. Chemical components, especially reactive species in cold atmospheric plasma (CAP), are considered crucial in the biological response of cells and tissues to both direct and indirect treatments [5,6]. In addition, EM waves emitted by plasma are important to consider. Glioblastoma multiforme (GBM) is the most aggressive and prevalent primary brain cancer in adults, characterized by rapid growth and

infiltration into surrounding brain tissue, leading to a poor prognosis with a median survival of 12–15 months despite advanced treatments. To treat GBM non-invasively an innovative approach such as plasma discharge tube (PDT) generating EM waves offer promising avenues for GBM therapy. While the concept remains similar to CAP, focusing more on physical treatment than the direct chemistry of reactive oxygen species (ROS), PDT involves partially ionized gas that focus on physical treatment utilizing EM waves generated by such plasmas. EM waves selectively induce oxidative stress in cancer cells, triggering apoptosis and inhibiting proliferation [7,8]. Recent advances in CAP technology have demonstrated significant potential for cancer therapy through the

E-mail addresses: vik1808@gwu.edu (V. Soni), lilin@email.gwu.edu (L. Lin), anmol035@gwu.edu (A. Taploo), js3853@rwjms.rutgers.edu (J.H. Sherman), keidar@gwu.edu (M. Keidar).

^{*} Corresponding author.

^{**} Corresponding author.

¹ Equal contribution.

generation of RONS that can selectively induce oxidative stress and apoptosis in tumor cells while sparing normal tissues [1-8]. Various plasma delivery configurations such as dielectric barrier discharges (DBDs) and plasma jets have been explored for biomedical applications, including glioblastoma treatment. However, most existing systems rely on open plasma exposure, limiting control over uniformity, reproducibility, and temperature regulation during treatment. Moreover, CAP jets and DBDs differ from the PDT in both emission characteristics and controllability. For example, Bekeschus et al. (2018) compared a floating-electrode DBD and kINPen jet and reported distinct plasma parameters and biological responses depending on discharge configuration. Xaubet et al. (2025) demonstrated that reactive species composition and temperature vary significantly across plasma jet devices, highlighting the dependence of chemical output on device geometry and gas flow. In contrast, the PDT is a closed system, confining plasma within a dielectric tube [9,10]. This design minimizes direct plasma medium contact and allows precise control over EM wave emission, making PDT primarily a physical treatment platform characterized by tunable electromagnetic fields with secondary, indirect RONS generation. However, the potential role of physical factors in cold plasma has often been overlooked, primarily due to the lack of direct experimental evidence showing cellular responses [11,12]. Building on our previous studies demonstrating the anticancer potential of PDTs and cold plasma plus TMZ combinations (Gjika et al., 2020; Murphy et al., 2025), the present work provides an extensive physical and electrical characterization of a closed PDT [13-15]. The primary focus of this study is on the physical EM field effects generated by the PDT, while the reactive species chemistry is considered a secondary downstream mechanism arising from EM-induced cellular responses. The PDT confines plasma within a dielectric tube while emitting EM waves and reactive species capable of penetrating biological barriers. This study uniquely investigates the fundamental plasma physics underlying non-invasive plasma-based cancer therapy, which had not been explored in earlier reports. Research shows that EM waves can stimulate the generation of ROS by interacting with biological molecules, leading to oxidative stress and inhibit cancer [16-20]. While the cold PDT may not directly generate ROS or induce chemical reactions as its primary effect, the physical factors associated with PDT can trigger an increase in endogenous ROS production in cells. This rise in ROS levels occurs as a secondary effect of EM emissions, influencing cellular signaling and potentially leading to therapeutic outcomes or cellular damage. Although OES of the sealed PDT system indicated minimal gas-phase ROS/RNS emission, PDT exposure can still influence intracellular redox balance through EM stimulation. EM waves generated by the plasma are known to enhance endogenous ROS production, triggering oxidative stress and apoptosis in cancer cells. In our previous studies, we also observed a significant increase in intracellular ROS following PDT exposure, supporting the role of EM-induced oxidative signaling in mediating its anticancer effects [15,21]. The concept of tumor-treating fields (TTF) is akin to the EM waves produced by PDT, which enhance drug efficacy by modulating cellular responses, increasing membrane permeability, and enabling deeper penetration of therapeutic agents.

An advantage of PDT is that they operate as a closed system, which helps maintain consistent conditions and stability for generating CAP [22]. There is emerging evidence suggesting that EM waves can be effective in treating GBM. Research indicates that EM waves, such as those used in TTF, can disrupt cancer cell division and inhibit tumor growth by creating an electric field that interferes with the mitotic process [23,24]. Clinical studies have shown that TTF therapy can extend progression-free survival and overall survival in GBM patients when used in combination with standard treatments [25–28]. These findings highlight the potential of EM waves as a promising adjunctive treatment modality for GBM, offering a non-invasive option to enhance therapeutic outcomes. This combination of EM waves generated from PDT and various drugs like Elesclomol, Taxol, and TMZ, etc. holds the potential for improving therapeutic outcomes in GBM treatment by

leveraging their unique mechanisms of action against cancer cells. To date, no advanced characterization has been conducted on the physical effects caused by the cold PDT. This study represents the first comprehensive analysis of various plasma diagnostics in PDT.

2. Materials and methods

2.1. Radial PDT experimental setup

The PDT device utilized in this study was developed and fabricated at the MPNL of George Washington University (GWU), following previously published methods [29]. The PDT used in this study consisted mainly of a cylindrical quartz glass tube (ACS Pharma) filled with pure helium (99.995 % purity, Roberts Oxygen, grade 4.5, size 300). The discharge was initiated by two electrodes at a voltage of 5.8 kV and a frequency of 12.5 kHz (Fig. 1). The PDT system featured a cylindrical glass tube with dimensions of 8 cm in height, 4 cm in diameter at the center, and 2 cm at the neck, providing a tapered design that ensured uniform plasma discharge and efficient confinement of reactive species. A central stainless steel anode (0.25 cm radius, 10 cm length) provided a stable discharge point, while an annular cathode (2 cm radius, 2.5 cm height) positioned around the outer central region optimized electric field coupling and plasma streamer formation. This electrode configuration generated a symmetric electric field, enabling stable discharge propagation and efficient production of RONS and electromagnetic emissions for therapeutic applications. To prevent overheating, two 12 V DC cooling exhaust fans (GOSTIME) were installed on both sides of the apparatus (Fig. 1). The operating conditions and geometric dimensions of the PDT are summarized in Table 1.

2.1.1. Comparison with existing plasma systems and advanced features of the PDT

The PDT system used in this study differs significantly from conventional plasma delivery configurations such as cold plasma jets or DBD systems. Unlike open plasma jets that require direct gas contact with tissues, the present PDT operates as a non-invasive, closed system, with plasma fully contained within a quartz tube. This configuration allows EM waves and plasma-generated species to propagate through biological barriers, including tissue and bone, without direct plasma tissue interaction. The design also ensures a uniform electric field distribution, preventing local thermal hotspots and maintaining

Table 1
Operating conditions of the PDT.

Parameter	Description
Tube Length	8 cm
Tube Diameter	4 cm (center), 2 cm (neck)
Electrode Configuration	One electrode connected to DC output; opposite copper electrode grounded
Annular Electrode (Cathode) Dimensions	2.5 cm width \times 18 cm length, 2 cm radius
Annular Electrode Function	Wrapped around outer tube surface to provide uniform conductive coverage
Inner Nail Electrode (Anode) Dimensions	0.5 cm thickness \times 10 cm length
Inner Nail Electrode Function	Axially positioned high-voltage electrode for plasma discharge
Applied Voltage	10 V
Discharge Frequency	12.5 kHz
Gas Type and Purity	Helium, 99.995 % (Roberts Oxygen, grade 4.5)
Gas Flow Rate	4 L/min (pre-filling, tube sealed; no flow during treatment)
Treatment Duration	1,4,7 min
Culture Plate Type	96-well plate or 35 mm petri dish
Gap Between Tube and Plate	0 cm (direct contact with tube)
Orientation of Tube	Upright, with the Petri dish or well plate positioned flat on top
Maximum PDT Temperature after treatment	32.4–35.1 °C after 7 min (below 37 °C culture temperature)

operational temperatures below 37 $^{\circ}$ C, thereby preserving the non-thermal characteristics of the discharge.

Furthermore, the system is scalable and adaptable for various clinical configurations, including wearable or helmet-based formats designed for targeted glioblastoma therapy. These structural and operational features collectively enhance the precision, safety, and translational potential of the PDT compared to existing plasma systems [29,30].

2.1.2. Device design and Fabrication

The PDT device was constructed using a quartz dielectric tube housed within a 3D printed support frame fabricated from polylactic acid (PLA), a biocompatible and thermally stable polymer. The PLA frame was designed to securely position the electrodes and maintain precise alignment of the plasma tube during operation while ensuring electrical insulation and mechanical stability. The materials used in the PDT assembly, including the quartz glass, medical grade silicone insulation, and PLA frame, were selected for their biocompatibility, chemical inertness, and suitability for future translational applications. Although the present work did not focus on new material development, the modular 3D printed structure allows easy customization of the PDT geometry for preclinical and patient specific device configurations.

2.2. Measurement of electric potential

Electric potential distribution across the PDT was measured using a high-impedance differential probe (Tektronix P6015A) connected to a digital oscilloscope (Tektronix TBS2204B). The probe tips were carefully positioned along the top surface of the PDT tube at incremental radial distances (center, mid-point, and edge) to capture spatial variations in potential. The measurements were performed under standard operating conditions (10 V, 12.5 kHz) with helium gas pre-filled and sealed inside the tube. Each measurement was repeated five times to ensure reproducibility, and mean values were calculated after background subtraction.

The resulting data revealed a gradual decrease in electric potential from the central axis toward the radial edge of the tube, consistent with the expected field decay across the dielectric surface (Figs. 1, 4–7). This gradient reflects both electrode geometry and the dielectric constant of the glass tube, which together shape the internal plasma confinement and external EM field distribution. For calibration, the oscilloscope was first zeroed using a grounded copper plate in place of the PDT to eliminate environmental noise and verify baseline stability. The obtained potential profiles were later correlated with near-field E-field and H-field measurements to provide a comprehensive picture of electromagnetic energy distribution within the system.

2.3. Optical emission spectroscopy (OES) spectra measurement

OES analysis of the PDT was performed using a SpectraWiz® spectroscopy system, with both the spectrometer and detection probe obtained from Stellar Net Inc. (Tampa, FL, USA, StellarNet EPP2000). The optical probe was positioned above and at the side of the PDT region, and spectral data were collected with an integration time of 1 s. The UV visible NIR spectrum (200–850 nm wavelength range) was analyzed to identify the species composition generated within the PDT. Emission features corresponding to various RNS and ROS, including nitrogen (N2; second positive system), nitrogen cation (N½; first negative system), nitric oxide (NO), atomic oxygen (O), and hydroxyl radicals (OH), were identified under dark conditions as previously described [31–36]. The distinction between N2 and N½ emission bands was maintained, as they represent different excited nitrogen states relevant to plasma diagnostics [37].

2.4. Chemicals and drugs

Elesclomol (STA-4783; SML2651), Paclitaxel (Taxol; 33069-62-4),

and Temozolomide (TMZ; T2577) were obtained from Sigma-Aldrich (St. Louis, MO, USA). All drugs were dissolved in dimethyl sulfoxide (DMSO) to prepare stable stock solutions for in vitro assays, followed by dilution in the respective culture medium to reach the desired final concentrations. The final DMSO concentration in all in vitro assays was maintained at 0.25 %, a level widely reported to be non-cytotoxic to mammalian cell lines, including cancer cell cultures [38–40]. Consistent with these reports, our control viability assays confirmed that 0.25 % DMSO did not significantly affect cell survival across the tested cell lines. The half-maximal inhibitory concentration (IC $_{50}$) of each drug was determined individually for every cell line. Subsequent in vitro treatments were performed by adding the drugs to the culture medium at final concentrations corresponding to their respective IC $_{50}$ values in Minimum Essential Medium (EMEM) or Dulbecco's Modified Eagle Medium (DMEM) at the time of treatment.

2.5. Cell lines and Cell culture

Human GBM cell lines A-172, T98G, and U-87 MG were procured from the American Type Culture Collection (ATCC). A172 cells were cultured in DMEM while U-87 MG and T98G were cultured in EMEM supplemented with 10 % fetal bovine serum and 1 % penicillinstreptomycin. All cultures were incubated at 37 $^{\circ}\text{C}$ in a humidified atmosphere containing 5 % CO₂.

2.6. Cell viability assay using PDT treatment In vitro

Cells were detached using 0.25 % trypsin-EDTA and seeded in 96-well tissue culture-treated microplates or 35 mm petri dishes at a density of 5 \times 10 3 cells per well and 1 x 10 4 cells per dish. The cells were cultured in complete DMEM medium. After 24 h of incubation for cell adherence, the media was replaced. They were washed with PBS, and were treated with PDT for 1,4, and 7 min. Subsequently, cells were further incubated at 37 $^{\circ}\text{C}$ for 72 h. Cell viability was assessed using an MTT and CCK8 assay. Absorbance was measured at 570 nm using a Synergy H1 hybrid multi-mode microplate reader.

2.7. In vitro PDT treatment setup

Cells were seeded in 35 mm petri dishes (1 \times 10⁴ cells per dish) or 96-well plates (5 \times 10³ cells per well) and positioned directly on top of the PDT during treatment, resulting in a distance of 0 cm between the plasma and the cell culture surface. The PDT is a fully enclosed system; therefore, no continuous gas flow was applied during operation. Prior to plasma activation, the quartz tube was filled with helium gas at a flow rate of 4 L/min for 8 min. The gas inlet was then disconnected, and the tube was sealed with a rubber cork to retain the gas. Plasma was subsequently operated at 12.5 kHz and 10 V, with the tube oriented vertically and the culture plates placed flat on top. Untreated controls were included by placing the cells on top of the PDT without activating the plasma discharge, effectively reproducing a helium-only exposure in the absence of reactive plasma species. This configuration ensures that the observed biological effects arise solely from plasma-generated reactive species and electromagnetic fields, rather than from helium gas or other external factors. The temperature of the culture medium was continuously monitored and remained below 37 °C throughout the exposure period, confirming the non-thermal nature of the treatment. A schematic representation of the in vitro PDT setup, including tube orientation and plate positioning, is shown in Fig. 1A and B.

2.8. Statistical analysis and data presentation

All quantitative data are expressed as mean \pm SEM, derived from at least three independent biological experiments and multiple independent biological replicates (n = 16 total per condition). Error bars representing SEM are included in all figures displaying percentage cell

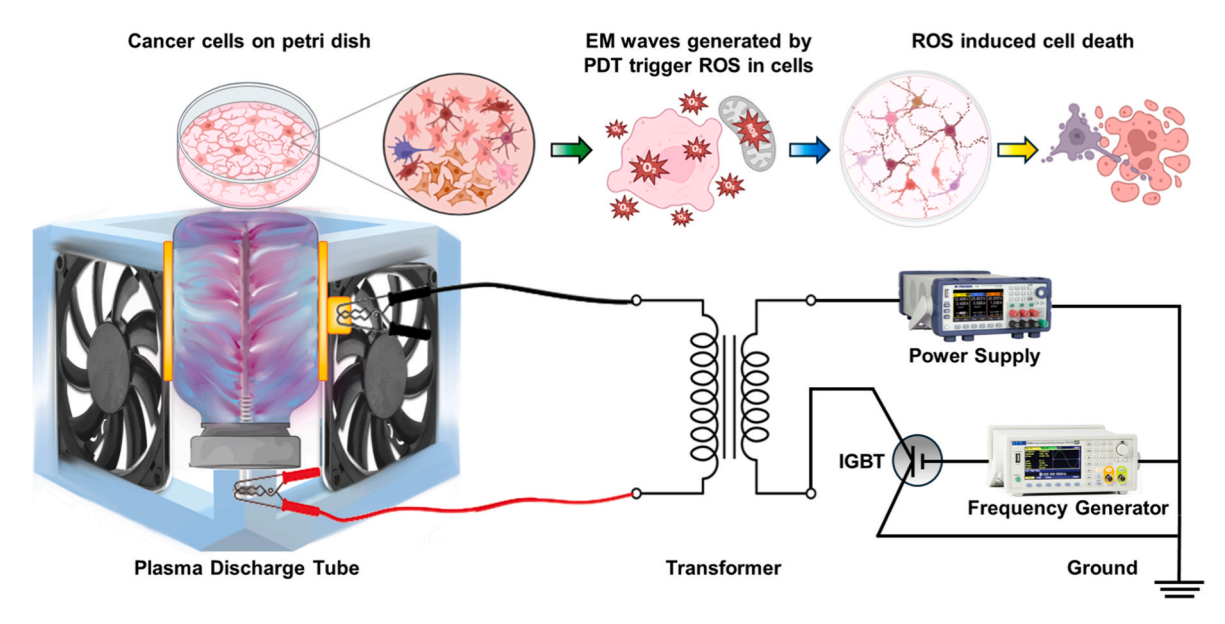


Fig. 1A. Schematic of the PDT system showing plasma streamer formation, circuit configuration, and EM wave emission leading to cell inhibition.

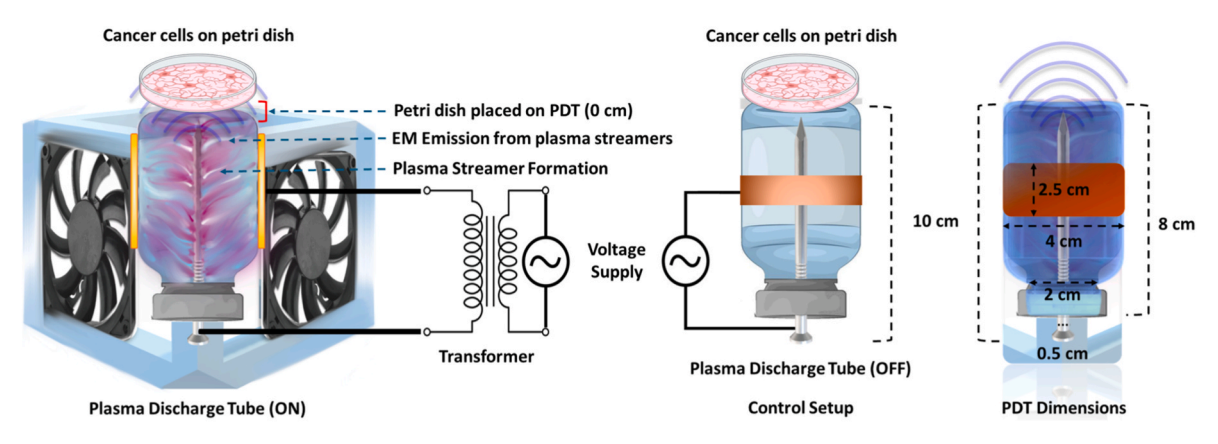


Fig. 1B. Schematic of the PDT system and in vitro treatment setup. Cells were seeded in Petri dishes and positioned directly above the PDT, corresponding to a 0 cm distance between the plasma source and the cell layer. Untreated control samples were placed under identical conditions without plasma activation, representing helium-only exposure. To the right, the PDT dimensions are shown: the tapered glass tube (8 cm height, 4–2 cm diameter) contains a central stainless steel anode and an outer annular cathode, forming a symmetric electric field for stable plasma discharge and RONS generation.

viability and related quantitative outcomes. Statistical analyses were performed using one- or two-way ANOVA followed by Dunnett's or Tukey's post hoc multiple comparison tests, as appropriate. Statistical significance was set at p < 0.05. Levels of significance are denoted in the figures as follows: p < 0.05 = *, p < 0.01 = ***, <math>p < 0.001 = ****, p < 0.001 = ****, p < 0.001 = ****, and ns = not significant. Exact <math>p-values are reported in the corresponding Supplementary Tables 1–3. All analyses and graph generation were performed using GraphPad Prism version 8.4.3 (GraphPad Software, San Diego, CA, USA).

3. Results

3.1. PDT setup and measurement of OES

Operation of the PDT system resulted in the consistent generation of bright, well-defined plasma streamers within the quartz chamber (Fig. 1). Upon helium gas flow (99.995 % purity), the system produced a stable and uniform glow discharge, with visible filamentary structures extending throughout the volume of the tube. These streamers displayed dynamic branching behavior and appeared to propagate symmetrically from the central anode toward the outer cathode, confirming effective ionization and energy distribution within the system. Thermal stability

was maintained throughout extended operation, with no visible signs of overheating or performance degradation, indicating the cooling mechanisms were effective. The system also demonstrated reliable ignition and repeatability of discharge across multiple trials, suggesting robust electrical performance and consistent plasma formation. These observations validate the PDT design for controlled plasma generation and support its suitability for downstream biological and therapeutic applications.

The OES analysis of the PDT was conducted to identify reactive species within the wavelength range of 300–800 nm. The analysis highlighted distinct peaks associated with ROS and RNS as mentioned in Fig. 2A–D. These peaks are indicative of the specific wavelengths at which these species emit radiation, providing valuable insight into the plasma's chemical environment. Fig. 2C presents a plot of discharge power versus frequency, showcasing various peaks corresponding to different frequencies of the plasma discharge. This plot reveals the frequency characteristics of plasma within the PDT, illustrating how discharge power varies with frequency and providing a deeper understanding of the plasma's operational parameters.

Fig. 2D displays the intensity ratio analysis of the plasma discharge. The data indicates that the lowest intensity ratio is observed around the frequency of $12.5~\rm kHz$ and $11.5~\rm kHz$. The maximum was seen at $16.5~\rm kHz$

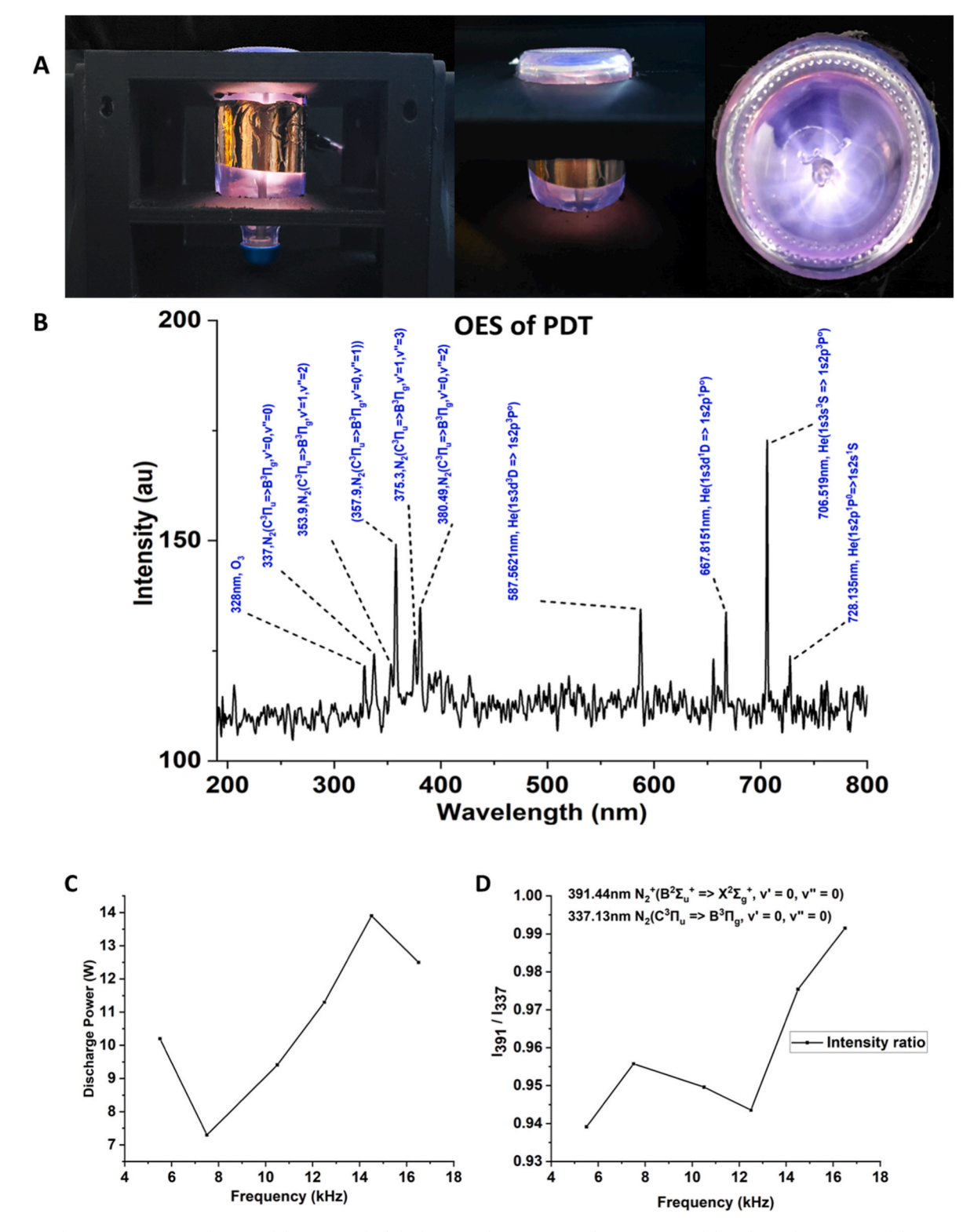


Fig. 2. PDT Analysis (A) presents a side view of the PDT on the left, depicting the structure and arrangement of the tube, and a top view of the PDT on the right, offering a comprehensive view of the tube's configuration and the placement of the optical probe. The optical probe was strategically positioned on the top and sides of the discharge tube for measurements. In (B), the OES analysis of the PDT is depicted, highlighting peaks indicative of ROS and RNS within the wavelength range of 300–800 nm. (C) Illustrates the observation of different discharge power versus frequency plot peaks, providing insights into the frequency characteristics of the plasma discharge within the PDT. Finally, (D) showcases the intensity ratio analysis, revealing that the lowest intensity ratio is observed around the frequency of 12.5 kHz.

kHz. This finding suggests that at this particular frequency, the ratio of emitted intensities is minimized, which could have implications for optimizing plasma conditions for specific applications.

3.2. High-speed imaging of PDT

Next, we performed high-speed camera imaging of the radial PDT. The high-speed camera imaging of the radial PDT captured dynamic emissions and streamers at specific time intervals. Notably, maximum emissions were observed at $t=9,\,10,\,$ and $11\,$ µs, indicating intense plasma activity and light emission during these moments. Additionally, emissions at $t=12,\,14,\,$ and $18\,$ µs highlighted the temporal evolution and propagation of plasma streamers within the discharge tube (Fig. 3).

This detailed temporal analysis provides critical insights into the transient behavior and dynamics of the plasma discharge, aiding in the understanding and characterization of the PDT's operational characteristics and performance.

3.3. Electromagnetic emission measurements

Next, we progressed to explore the emission characteristics of a radial PDT through EM emission measurements. This investigation involved the utilization of two WR75 horns for emission detection. Our findings unveiled multiple distinct peaks within the gigahertz (GHz) range, specifically at frequencies of 16.3 GHz, 16.6 GHz, and 17.7 GHz from the radial PDT (Fig. 4A and B). These peaks observed in the

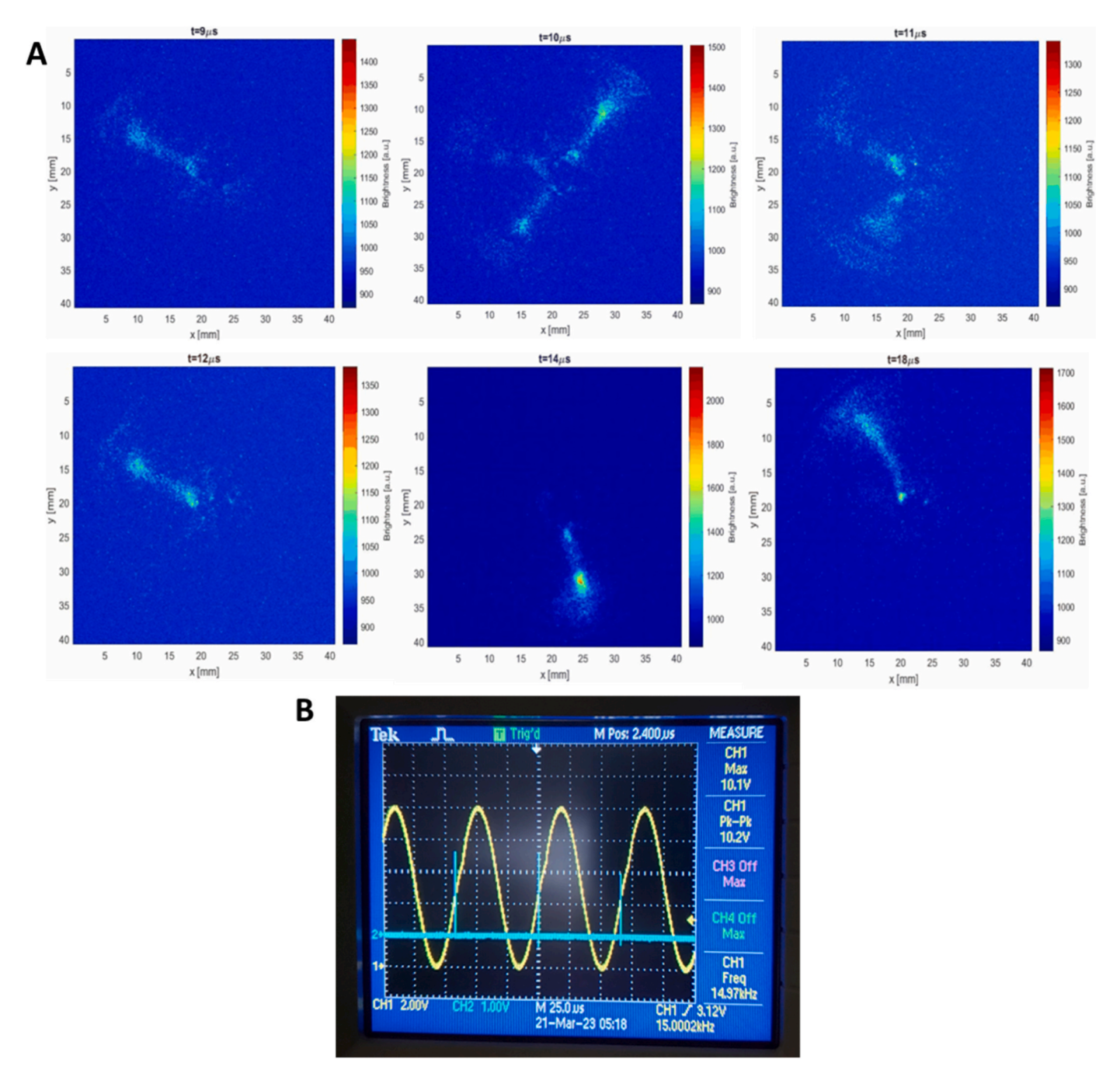


Fig. 3. (A) High-speed camera images of the radial PDT showing dynamic emissions and streamers over time. Peak emissions are observed at t = 9, 10, and 11 μ s, indicating intense plasma activity. Temporal evolution and streamer propagation are highlighted at t = 12, 14, and 18 μ s. (B) Oscilloscope reading. This analysis reveals the transient behavior and dynamics of plasma discharge, enhancing understanding of PDT performance.

microwave power spectrum indicate the emission of EM waves within this frequency range. This exploration of EM wave emissions from the PDT aligns with previous research demonstrating the potential applications of microwave frequencies in cancer therapy. The interaction between EM radiation and biological tissues has garnered interest due to its ability to selectively target and affect cancer cells while minimizing damage to healthy tissues [41]. Furthermore, studies have shown promising results in utilizing microwave radiation for cancer treatment, such as microwave ablation and hyperthermia, which exploit the thermal effects induced by EM waves to destroy cancer cells [17,23,27,28].

3.4. Rayleigh Microwave Scattering (RMS) of PDT

In our study, RMS of the radial PDT was also performed. We observed multiple peaks in electron density measurements under specific experimental conditions. For the case with a vertical placement axis and a frequency of 14.5 kHz at 6V, the electron density peaked at 2.9×10^{11} electrons/m 3 . Similarly, with a horizontal placement of the PDT under the same frequency (14.5 kHz) and voltage (6V), the maximum electron density observed was 2.6×10^{11} electrons/m 3 (Fig. 4C and D). These results highlight the sensitivity of RMS in detecting variations in electron density within the PDT under different orientations and experimental settings, providing valuable insight into the plasma characteristics and behavior.

3.5. Estimation of emissions and harmonics using near field probes

PDT improves upon traditional CAP by enabling non-invasive treatment, eliminating the need for direct contact between the target tissue and the plasma. PDT works by generating an EMF through plasma irradiation, which is then projected onto the target cells. EMF generation in the MHz range arises from ion oscillations, whereas GHz-range emissions are attributed to fluctuations in electron density. The PDT is powered using a high-voltage, transformer-based alternating current (AC) circuit, which boosts the voltage from 10 V up to 5-10 kV peak-topeak at 12.5-15.5 kHz to initiate electrical breakdown in a helium-air gas mixture. These operating conditions were selected to maximize the production of RONS, as determined by OES. Previously, microwave (GHz-range) emissions were detected using a heterodyne setup for RF power spectrum analysis [29,36]. However, emissions in the Hz-kHz range had not been studied. In this work, we employ near-field probe antennas to detect and characterize the electromagnetic fields in this previously unexplored frequency range (Fig. 5) [42,43].

The probes were carefully calibrated using the PDT setup. First, the PDT was operated without helium gas, and the frequency was applied via a function generator at 10.5, 12.5, 14.5, and 16.5 kHz under the same voltage as plasma operation. The near-field probes were positioned in the setup, and background signals were recorded to remove noise. Oscilloscope readings confirmed that detected peaks matched the generator frequencies, validating probe functionality (Fig. 5C). The PDT

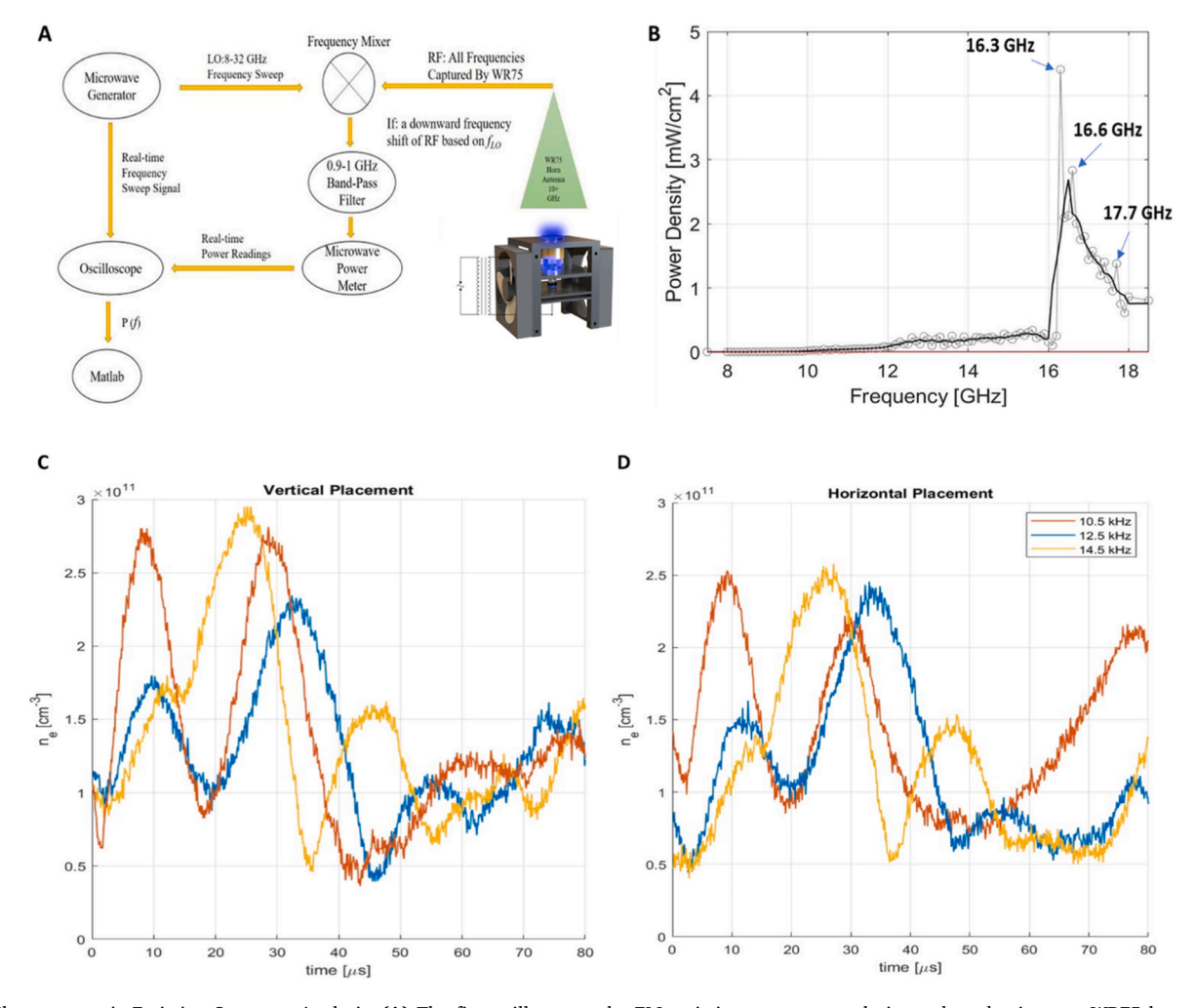


Fig. 4. Electromagnetic Emission Spectrum Analysis. (A) The figure illustrates the EM emission spectrum analysis conducted using two WR75 horns to detect emissions from a radial PDT. (B) The spectrum analysis revealed distinct peaks at specific gigahertz (GHz) frequencies, notably at 16.3 GHz, 16.6 GHz, and 17.7 GHz. These peaks signify the emission of EM waves within the microwave power spectrum range by the radial PDT. (C, D) RMS measurements showing electron density peaks in the radial PDT under specific experimental conditions.

was then filled with helium, and plasma discharge was activated to measure Electric (E)— and magnetic (H)-fields, including harmonics. Measurements were taken with and without the PDT active, and background noise and harmonics were subtracted to isolate the PDT contribution. The confirmed EM frequencies validated both probe and amplifier performance. To ensure accurate EM field measurements, all EMF, and near-field probe readings were performed in triplicate (n = 3 per group) and are presented as mean \pm SEM. The handmade H- and Efield probes followed IEC 61000-4-9 geometries and were calibrated against reference signals prior to measurement. The oscilloscope's internal calibration and amplitude accuracy (± 2 %) yielded an overall uncertainty of ± 1 dB (k = 2). Measurement errors were estimated at ± 2 –5% for near-field probes.

Depending on the probe design, it can detect electric fields, magnetic fields, or both. Understanding them separately helps us know if the EM wave is E or H-field dominant. Two cases were explored here (shown in (Fig. 5). One where the ground electrode is attached around the tube at the top vs middle. The goal was to obtain optimum conditions for the electrode positioning to maximize the EM emissions. As seen in Fig. 5A, an RF amplifier [42] was utilized to amplify the incoming plasma generated EM signal. The amplifier output was connected to an

oscilloscope to collect data. The oscilloscope was set to Fast Fourier Transform (FFT) mode to analyze the E-H field voltage in the frequency domain. This allowed for the identification of the specific emission frequencies and magnitude measurements. The horizontal scale of the oscilloscope was set to 1 ms, 10 ms and 40 ms to obtain emissions from Hz-KHz range. Based on the obtained data, power of emission could be obtained as equation (1):

$$P = 10^{\frac{2V}{20}} / R \tag{1}$$

where P is emission power (nW), V is voltage (db), R is resistance (50 Ω). The voltage needs to be converted to linear scale before calculating power. Next, we performed near-field probe experiments to obtain EM emission intensity, frequency, and harmonics.

The near field probe was utilized to measure E and H field emissions in the case of cathode at the top vs middle of the PDT as seen in Fig. 5B. The results indicated emissions 15.5 kHz, 31 kHz, 32 kHz, 46.5 kHz, 47.5 kHz and 62 kHz, indicating the harmonics of the PDT's primary operational frequency. However, unexpected emissions such as 0.125 kHz, 0.25 kHz, 0.375 kHz, 0.5 kHz, 0.625 kHz, 0.75 kHz, 2.5 kHz, 3 kHz, 3.5 kHz, 5.5 kHz and 6 kHz were observed simultaneously Fig. 6A,B.

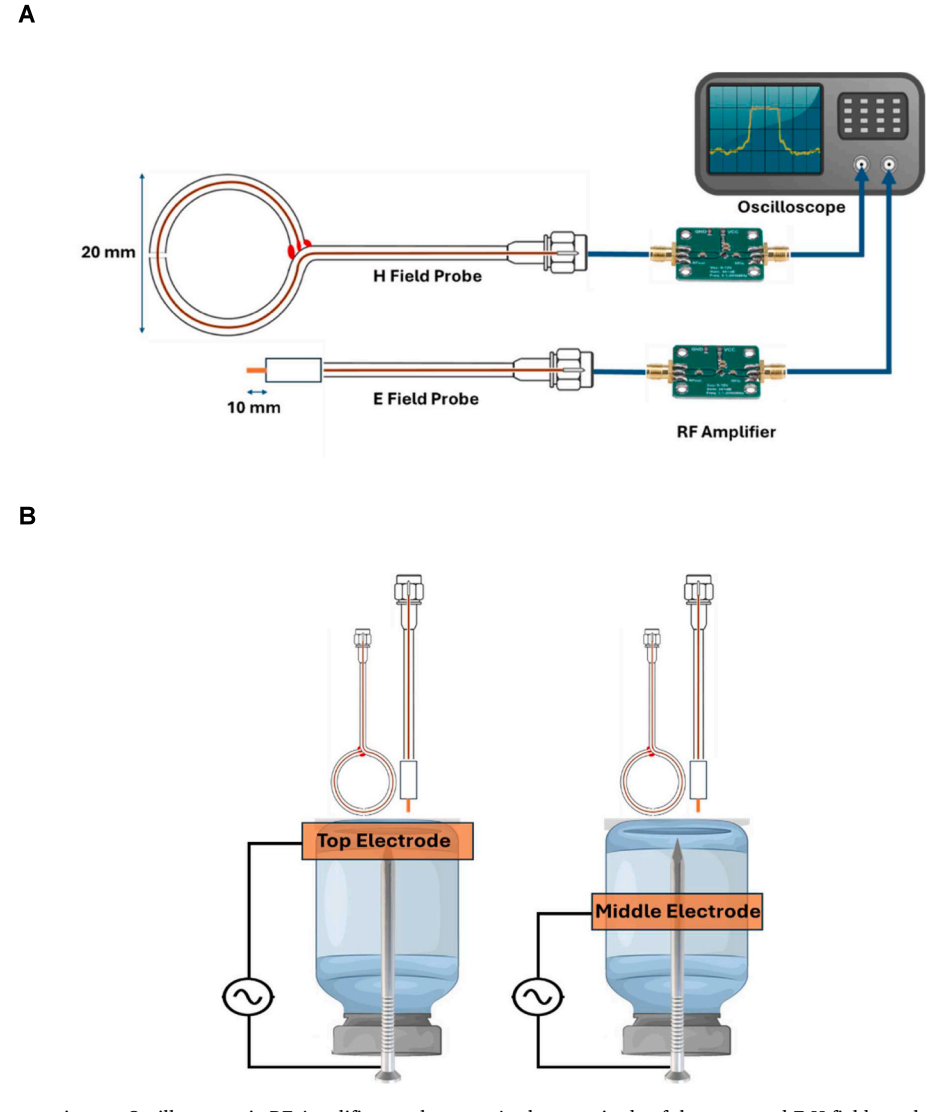


Fig. 5 (A). E and H field connections to Oscilloscope via RF Amplifier can be seen. As the magnitude of the measured E-H field was low, an amplifier was used to attenuate the incoming plasma generated EM wave signal. The diameter of the H field is 20 mm, and the length of the E field probe wire is 10 mm. (B) The probes were oriented above the PDT when the ground electrode was placed in top vs middle section. The probe measured the E-H field near field signal ranging from Hz-kHz harmonics.

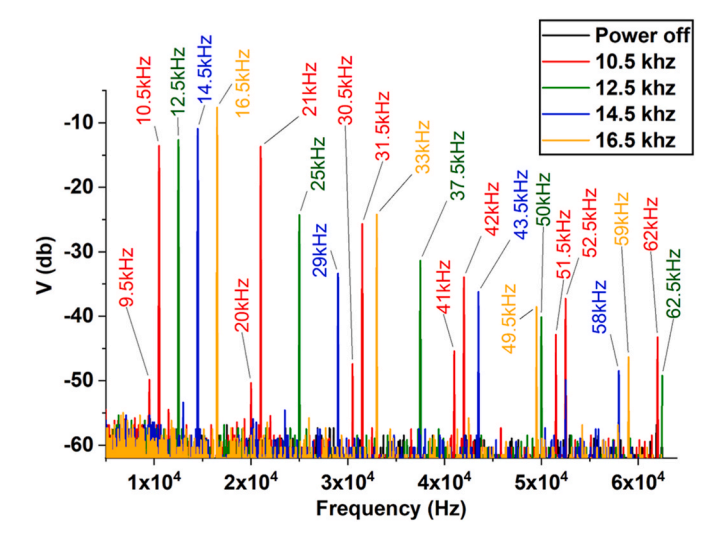


Fig. 5C. Calibration results of the near-field probes used for EM field validation in the PDT system when no helium gas was filled and the PDT was operated at reference frequencies (10.5–16.5 kHz). The function generator provided these frequencies to verify probe response and ensure signal accuracy prior to plasma discharge measurements, (n = 3 per group).

A possible explanation for this observation is that the emissions are strongly linked to the formation of multiple streamers or plasma bullets inside the discharge tube. The formation of these streamers is random, as seen in the ICCD camera images. This effect would not occur in the case of a single plasma jet, as it would produce only one plasma bullet. Nearfield probes were used to test the plasma jet, and as expected, the lower frequency peaks were absent, confirming the streamer interaction effect. The middle cathode configuration appears to produce more emissions compared to the top cathode configuration. This could be due to the larger plasma volume and the higher number of streamers. This effect is also reflected in the power calculations, which were derived using Equation (1) and shown in Fig. 6B. Strong emission can be seen for 0.125 kHz, 3 kHz and 15.5 kHz. No emissions were observed in MHz emission range. The middle cathode configuration exhibited greater emission of E-field power than the top cathode configuration. In the top cathode case, the plasma inside the PDT seems to be primarily concentrated in the top region, while in the middle cathode case, the plasma is more evenly distributed throughout the PDT. Additionally, the EM wave appears to be E field dominant in both cases as the impedance (E/H) is greater than 1. Although, EM generation/interaction from the plasma can be studied in detail using Ansys's high frequency structure simulator (HFSS)/COMSOL simulations, it is currently out of the scope of this research paper. Future work would also involve studying emissions as a function of device's operational frequency and voltage.

3.6. Estimation of E and H Fields Using a Three-axis EMF sensor

To accurately characterize the EM field emissions from the PDT, we employed a three-axis EM radiation tester (EMF01) equipped with an EM induction probe [43]. The sensor was positioned directly on top of the discharge tube, ensuring zero distance between the sensor and the plasma source for maximum field capture. This high-sensitivity instrument allowed simultaneous measurement of electric (E) fields in volts per meter (V/m) and magnetic (H) fields in microtesla (μ T), with a wide detection range of 5–2000 V/m for E-fields and 0.1–400 mG for H-fields. Measurements were taken in triplicates, with 10 readings per measurement session to reduce discrepancies and improve statistical reliability (Fig. 7). The EMF01's dual-mode LCD provided real-time visualization of E and H field intensities, and its data logging capability allowed for time-series capture and retrospective analysis of the emitted field spectrum. The EM induction probe utilizes advanced

sensing technology to detect both peak and average values, ensuring a comprehensive assessment of the EM environment surrounding the PDT.

Fig. 7 Shows EM field measurements using a three-axis EMF sensor for thin and thick electrode configurations. Panels (A) and (B) display H-field (μ T) and E-field (V/m) measurements for thin electrodes placed on top of the PDT, respectively. Panels (C) and (D) show the corresponding H-field and E-field measurements for thick electrodes placed in the middle of the PDT. This comparison demonstrates how electrode geometry affects electromagnetic field distribution in the experimental setup (n=10 per group). (E) shows a three-axis EM radiation tester (EMF01) equipped with an EM induction probe. (F) illustrates the PDT in operation following the measurement of E and H fields.

We tested two configurations by placing either a thin or a thick copper electrode on the PDT. For each electrode type, we measured the E and H fields at three different frequencies 12.5 kHz, 14.5 kHz, and 16.5 kHz while keeping the input voltage constant at 10 V. In the case of the thin electrode, the H field remained relatively constant across all frequencies, while the E field showed a gradual increase with rising frequency (Fig. 7A and B). Interestingly, the thick electrode exhibited the opposite behavior: the H field remained stable, while the E field reduced slightly with frequency compared to 12.5 kHz (Fig. 7C and D). These results highlight how electrode thickness and placement can significantly influence the electromagnetic field distribution, offering a potential method to fine-tune PDT-based cancer treatments by modulating field characteristics for targeted therapeutic outcomes.

3.7. Power density and thermal behavior of plasma discharge tube at varying frequencies

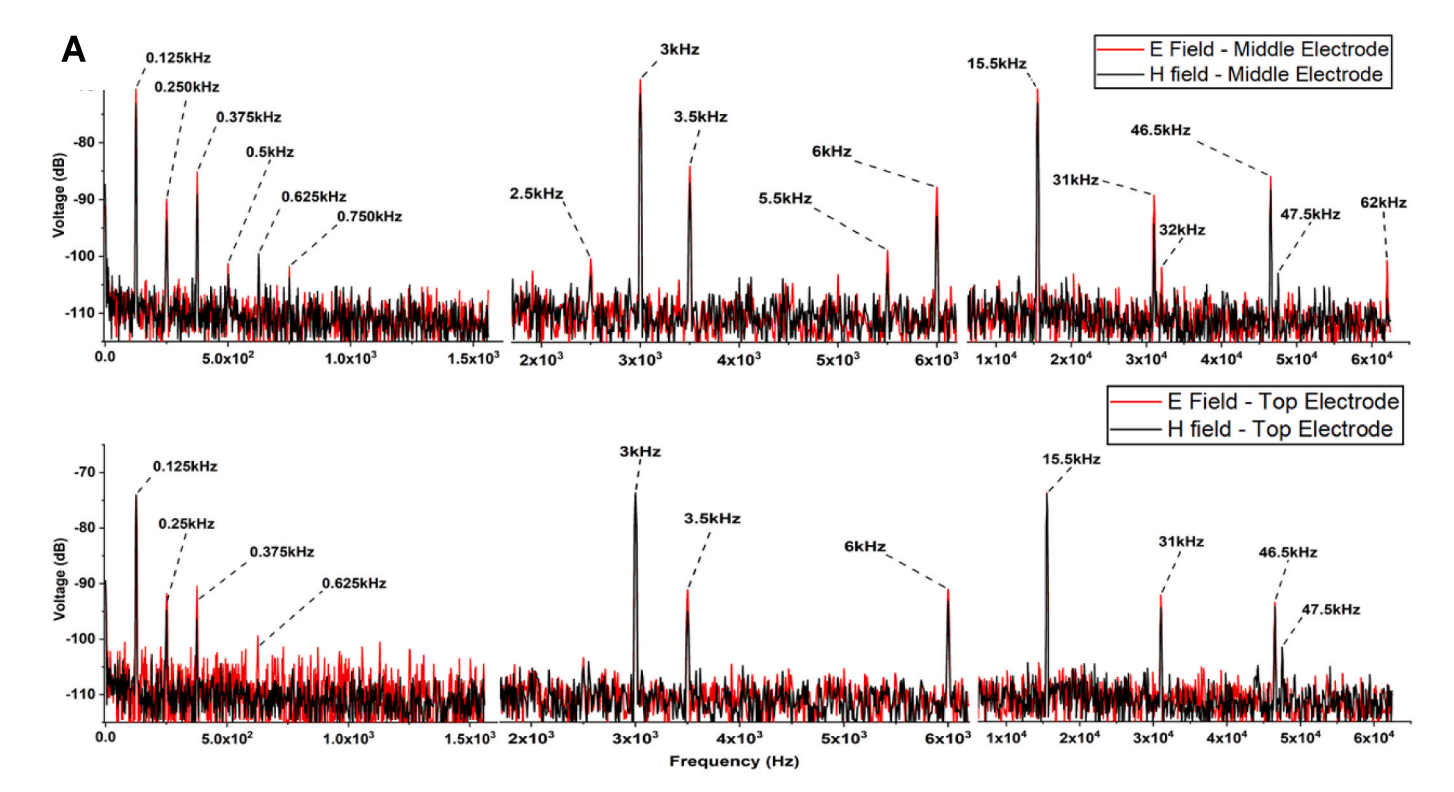
Next, power densities were calculated based on the measured E and H fields at three operating frequencies: 12.5 kHz, 14.5 kHz, and 16.5 kHz (Fig. 8). For the thin copper electrode placed at the top of the PDT device and operated at 10 V input, the power density increased with frequency, reaching a maximum at 16.5 kHz. Specifically, power densities were calculated to be 8.11×10^{-7} , 1.49×10^{-6} , and 3.38×10^{-6} W/m² at 12.5, 14.5, and 16.5 kHz, respectively, indicating enhanced field strength and energy delivery at higher frequencies Fig. 8A.

In contrast, for the thick copper electrode positioned in the middle of the PDT device, the highest power density was observed at 12.5 kHz, followed by a decline at higher frequencies. The power densities for this configuration were $1.57\times10^{-6}, 6.64\times10^{-7}, \text{ and } 7.66\times10^{-7}\,\text{W/m}^2$ at 12.5, 14.5, and 16.5 kHz, respectively. These results suggest that electrode geometry and placement significantly influence the spatial distribution of EM fields and energy transfer characteristics within the PDT system Fig. 8B.

Additionally, temperature measurements were conducted with the fan turned on to ensure thermal regulation during operation. The temperature remained within an optimal range of 25–45 $^{\circ}$ C across various distances, demonstrating effective heat management and thermal safety of the system. Power density measurements as a function of distance from the device showed a gradual decay, reflecting a corresponding decline in the E-field strength over distance Fig. 8C,D. This trend confirms the spatial attenuation of the EM field, which is critical for understanding the effective treatment range and optimizing device placement for therapeutic applications.

3.8. Enhanced cytotoxic effects of PDT in combination with Elesclomol (STA-4783), Taxol (paclitaxel), and Temozolomide (TMZ)

To further explore the therapeutic potential of the PDT, we evaluated its effects in combination with chemotherapeutic agents, including Eleschomol, Taxol and TMZ, in glioma cell models. Glioblastoma (GBM) was selected as a representative cancer type due to its highly aggressive nature, intrinsic therapeutic resistance, and poor clinical prognosis, which collectively underscore the urgent need for alternative treatment strategies. PDT offers a non-invasive modality capable of generating





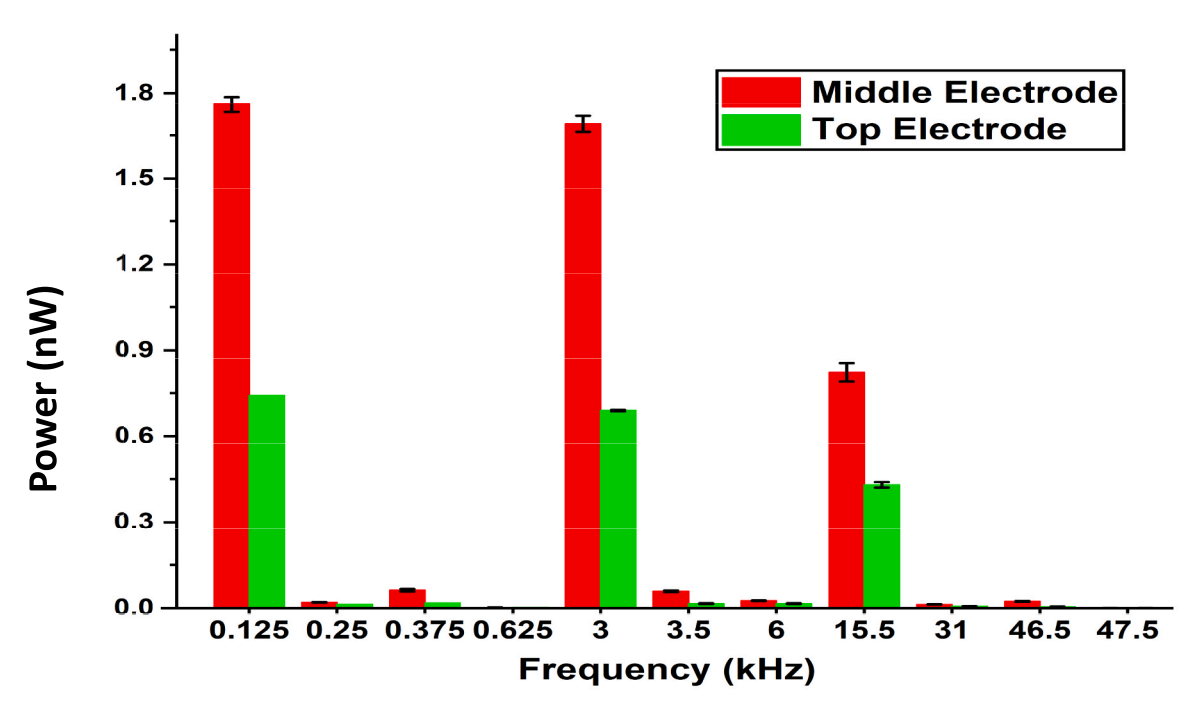


Fig. 6. (A) Measured FFT based E-H field emissions in the case where ground electrode was connected in the top vs middle of the PDT. The objective was to obtain the condition where emissions were greatest and check if the EM wave was E or H field dominant. (B) Power in nano watts was obtained from the emission lines in frequency ranging from Hz-KHz.

reactive species and EM effects that may potentiate the action of existing drugs. The rationale for combining PDT with chemotherapeutic agents was to determine whether this dual approach could overcome resistance mechanisms and improve therapeutic efficacy. Elesclomol, a copper-binding small molecule, induces oxidative stress through ROS

generation and triggers apoptosis, however, its limited permeability across the blood brain barrier (BBB) constrains its clinical utility against brain tumors. While Taxol disrupts microtubule dynamics and inhibits mitotic progression. TMZ, the current first-line therapy for GBM, alkylates DNA to induce cytotoxicity but often faces resistance due to DNA

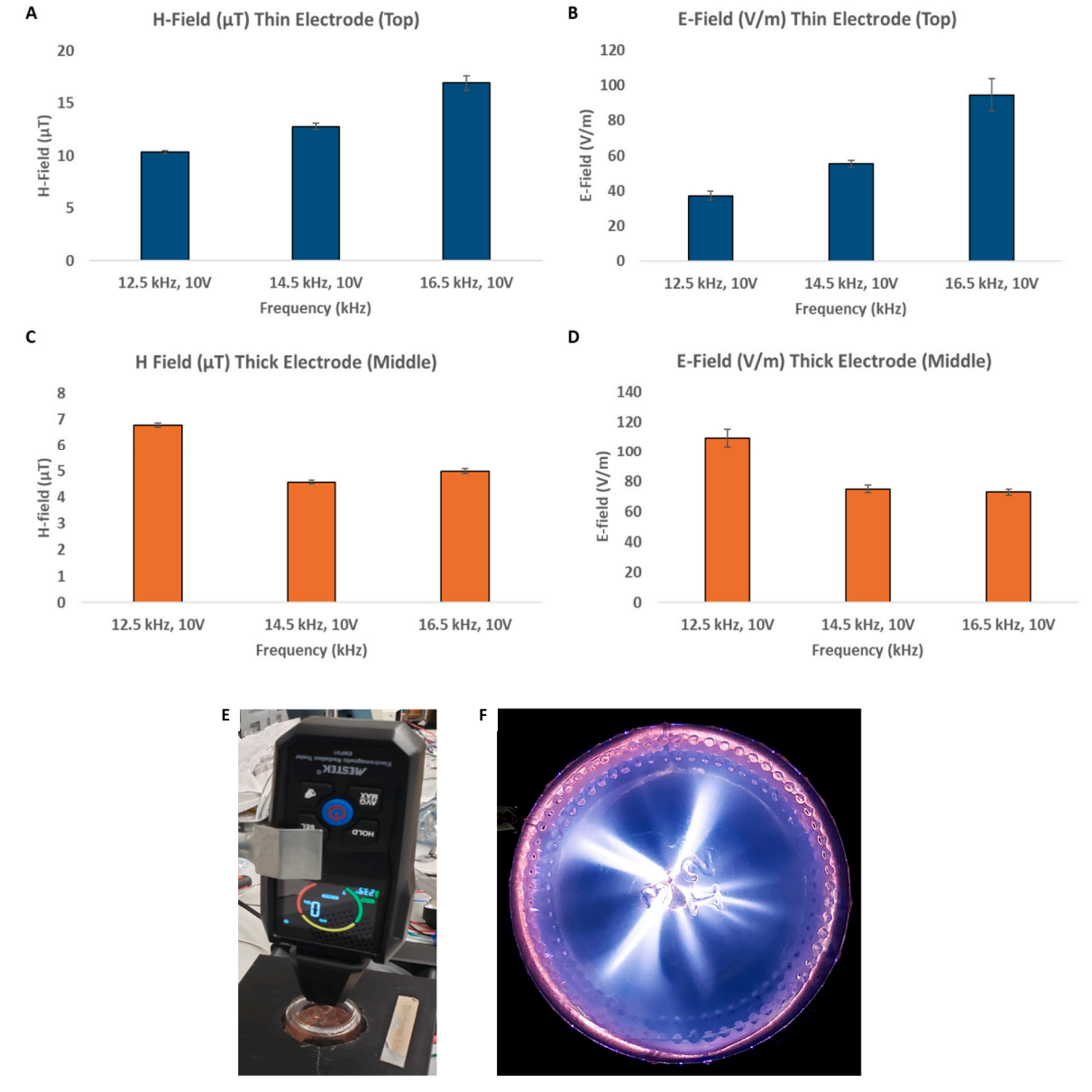


Fig. 7. Estimation of E and H fields using a three-axis EMF sensor.

repair mechanisms. Thus, combining PDT with Elesclomol, Taxol, or TMZ was hypothesized to enhance overall antitumor efficacy by integrating oxidative, cytostatic, and genotoxic mechanisms within GBM cells.

Elesclomol functions by binding to copper ions and generating ROS, which induce oxidative stress and trigger apoptosis in metabolically active cancer cells. Its cytotoxic effect primarily arises from disrupting the cellular redox balance. The half-maximal inhibitory concentration (IC $_{50}$) of Elesclomol (STA-4783) was determined to be 27.58 nM for A-172 cells, 54.20 nM for T98G cells and 77.05 nM for U-87 MG cells (Fig. 9A–C).

Taxol (Paclitaxel) is a well-established chemotherapeutic agent that exerts its cytotoxic effects by stabilizing microtubules and inhibiting their depolymerization, thereby disrupting mitotic spindle formation and inducing apoptosis. Although conventional Taxol exhibits limited penetration across the BBB, advanced formulations such as nanoparticle albumin-bound paclitaxel (Abraxane) have been developed to improve central nervous system delivery. The IC_{50} of Taxol in U-87 MG cells was determined to be 8.76 μ M (Fig. 9D).

In our previous studies, the IC₅₀ of TMZ was calculated for all three

GBM cell lines and was found to be higher than those of Elesclomol and Taxol. The IC $_{50}$ values for TMZ were approximately 125 μM for A172, 105 μM for U87-MG, and 247 μM for T98G cells [33–36]. Consequently, we limited PDT exposure to shorter durations (1, 2, and 3 min) when combined with TMZ to demonstrate that even brief PDT treatments can enhance the efficacy of TMZ in vitro.

3.9. Effect of PDT and drug combination treatments on Cell viability

To further evaluate the combinatorial potential of these agents, U-87 MG cells were treated with each drug in combination with PDT. The combined treatments produced significantly greater reductions in cell viability compared to either treatment alone, indicating that PDT exposure sensitized GBM cells to all three agents. Cell viability inhibition increased with PDT exposure time and was most pronounced when PDT was combined with Elesclomol, Taxol, or TMZ. For Elesclomol, at 1 min, inhibition was 15.2 % with PDT, 38.4 % with Elesclomol alone, and 49.9 % with PDT + Elesclomol, indicating that combining PDT with Elesclomol significantly enhanced cytotoxicity compared to either treatment alone. At 4 min, inhibition rose to 21.3 %, 43.9 %, and 50.7 %,

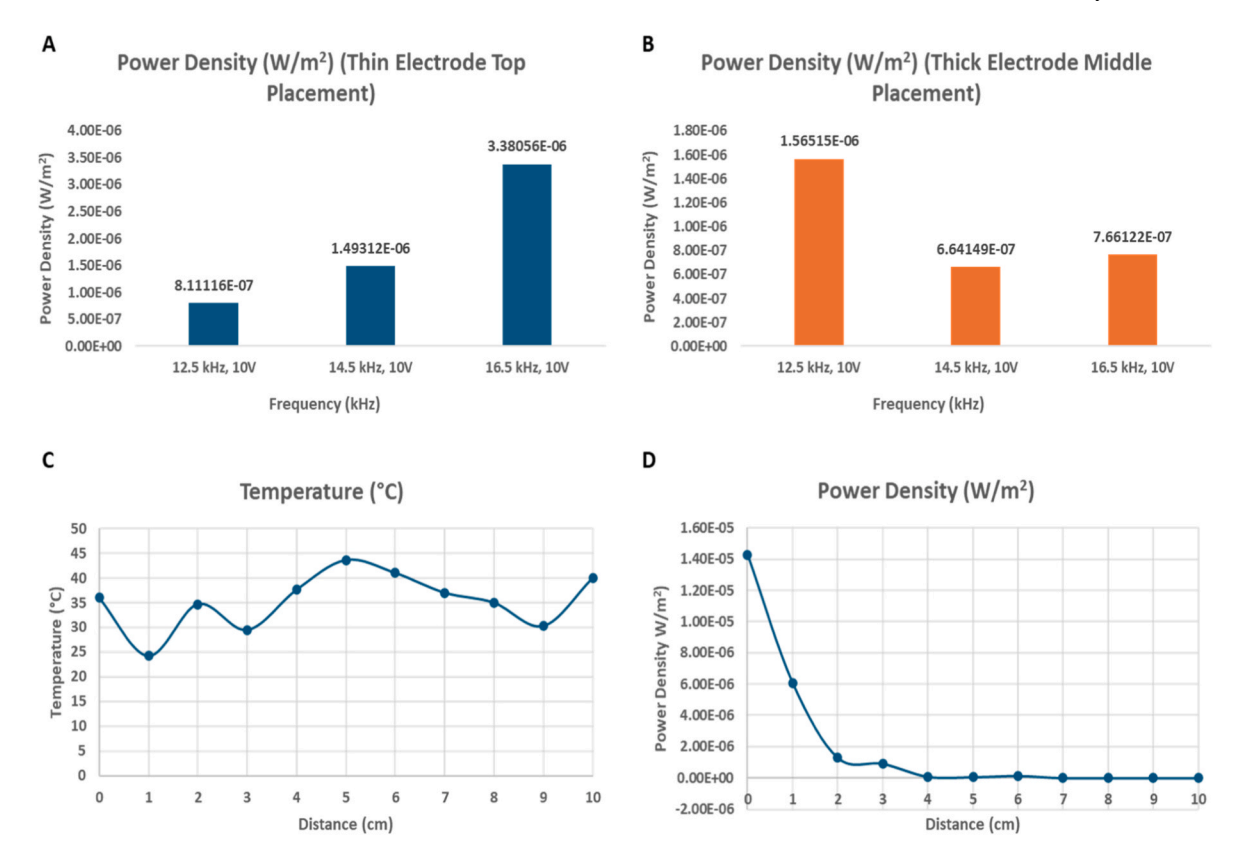


Fig. 8. Power density measurements at varying frequencies for both thin and thick electrodes positioned at the top and middle sections (A,B); temperature profiles of the PDT measured at distances up to 10 cm (C); and (D) corresponding power density calculations across the same distance range.

respectively, showing a further increase in cell killing with longer light exposure. At 7 min, inhibition reached 27.5 %, 41.2 %, and 52.5 %, confirming a strong time-dependent effect and suggesting that PDT augments Elesclomol's oxidative stress mediated cytotoxic response (Fig. 10 A-C). For Taxol, at 1 min, inhibition was 14.1 % with PDT, 66.1 % with Taxol alone, and 71.7 % with PDT + Taxol, demonstrating a clear additive effect. At 4 min, inhibition increased to 25.8 %, 66.9 %, and 72.9 %, showing that even with moderate PDT exposure, the combination produced higher toxicity than either agent alone. At 7 min, inhibition further increased to 36.2 %, 67.9 %, and 77.0 %, indicating strong inhibition and suggesting that PDT sensitizes cells to Taxolinduced microtubule disruption (Fig. 10 D-F). Similarly, for TMZ, at 1 min, inhibition was 22.8 % with PDT, 29.8 % with TMZ, and 40.5 % with PDT + TMZ, showing a noticeable enhancement of cytotoxicity. At 2 min, inhibition rose to 17.8 %, 35.9 %, and 45.4 %, and at 3 min to 19.7 %, 32.4 %, and 46.8 %, confirming that PDT in combination with TMZ consistently produced greater inhibition than either treatment alone (Fig, 10 G-I). Collectively, these results demonstrate that PDT markedly enhances the cytotoxic effects of Elesclomol, Taxol, and TMZ in a time-dependent manner, likely through mechanisms involving enhanced oxidative stress, mitochondrial dysfunction, and improved drug responsiveness in glioblastoma cells. Although combination treatments produced a modest additional inhibition (~7-10 %) compared to drug alone, statistical analysis confirmed that these differences were significant across multiple exposure times, supporting enhanced cytotoxic effect of PDT + drug co-treatment. Supplementary Table 1-3 summarize the detailed statistical outputs for U-87 MG cell viability after PDT treatment in combination with Elesclomol, Taxol, and TMZ respectively.

4. Discussion

Glioblastoma (GBM) is among the most aggressive and lethal brain

tumors, distinguished by marked heterogeneity and complex molecular signatures. While primary GBM arises de novo, secondary GBM evolves from lower-grade gliomas, each with differing genetic trajectories and treatment challenges [44,45]. Given this complexity, adaptive and personalized treatment strategies are essential. Our study introduces a novel, non-invasive PDT system capable of delivering tunable EM fields and reactive species tailored for GBM therapy.

The PDT system generates a unique combination of EM waves and plasma-derived RONS, which together contribute to its anticancer effects (Fig. 1). During discharge, oscillating electron avalanches produce radio-frequency EM fields that can penetrate biological tissue and modulate intracellular redox signaling. These EM fields have been reported to stimulate endogenous ROS production by perturbing mitochondrial electron transport and redox-sensitive membrane channels, including voltage-gated calcium channels and NADPH oxidase pathways [46,47]. In parallel, the sealed-tube plasma chemistry produces long-lived species such as H₂O₂, NO₂, and O₃, which diffuse to the cell surface and initiate oxidative stress [7,29]. Together, EM-induced endogenous ROS and plasma-generated exogenous RONS disrupt mitochondrial membrane potential, trigger cytochrome-c release, and activate caspase-dependent apoptosis [48]. In addition, elevated ROS levels cause oxidative DNA damage, including double strand breaks and base oxidation, ultimately activating ATM/ATR signaling and halting tumor cell proliferation [49–53]. Cancer cells are particularly vulnerable to this redox-mediated mechanism due to their higher basal ROS load and compromised antioxidant defenses, enabling PDT to selectively target tumor metabolism while sparing surrounding healthy tissue. Overall, the PDT mechanism leverages a combined physical and chemical modality, in which EM wave stimulation and RONS-driven oxidative stress converge on mitochondria and nuclear DNA to induce programmed cancer cell death.

Our results indicate that the PDT system is highly configurable, with its therapeutic performance modulated by parameters such as electrode

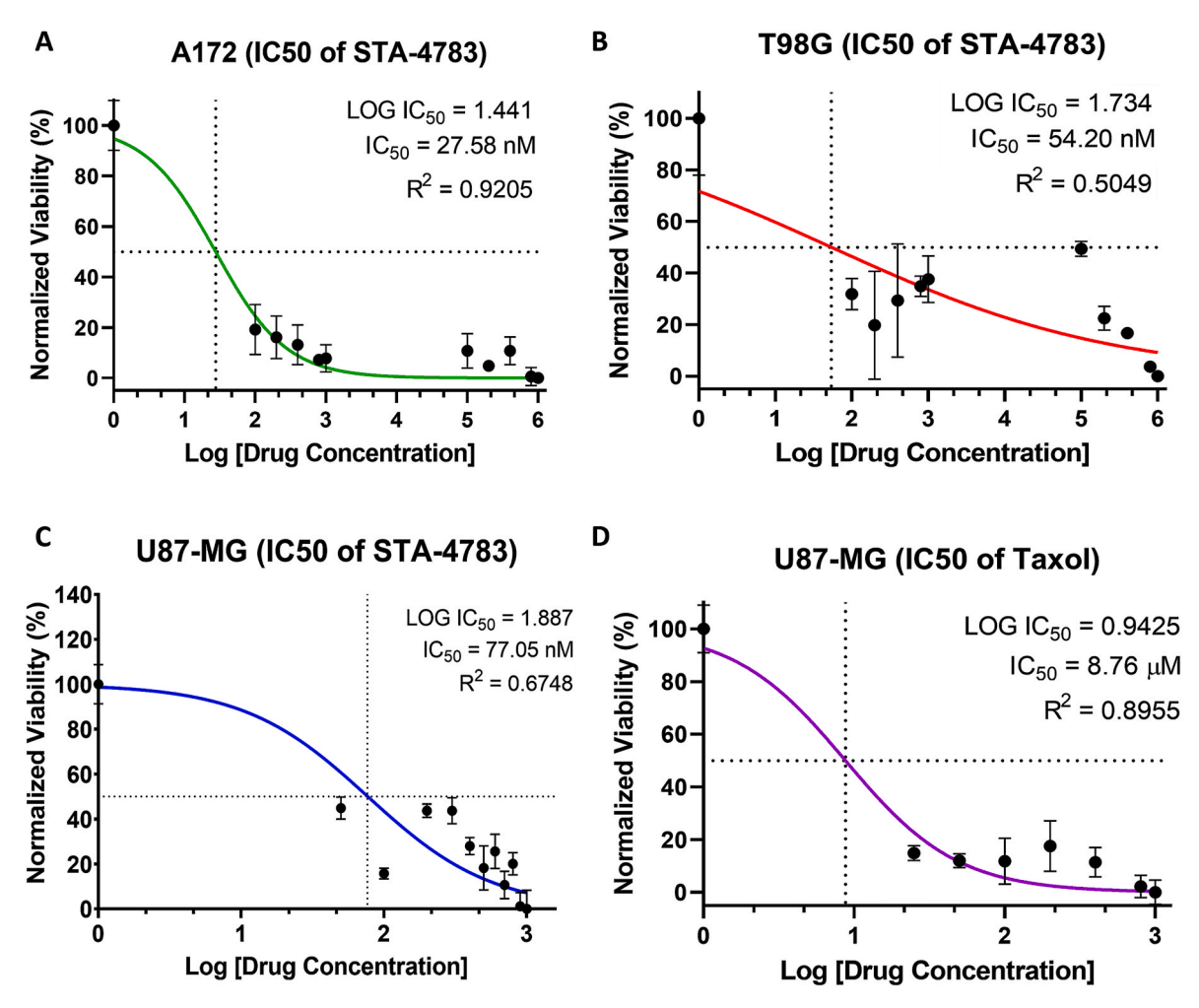


Fig. 9. Determination of IC_{50} values and dose response analysis of Elesclomol (STA-4783) and Taxol (Paclitaxel) in glioblastoma cell lines. (A–C) Dose response curves showing the IC_{50} of Elesclomol (STA-4783) in A-172, T98G, and U-87 MG cell lines, respectively. (D) IC_{50} of Taxol (Paclitaxel) in U-87 MG cells. Data represent mean \pm SEM from three independent experiments (n = 16 replicates per condition).

design, discharge frequency, and orientation. Importantly, OES of the PDT revealed consistent emission lines corresponding to RONS, including OH, N2*, and O lines (Fig. 2). These emissions are indicative of oxidative and nitrosative stress mechanisms central to cancer cell apoptosis. The emission intensity varied with both frequency and orientation, supporting our hypothesis that plasma composition and energy delivery can be tuned through physical parameters (Fig. 3). When comparing thin and thick copper electrodes across frequencies of 12.5, 14.5, and 16.5 kHz at 10V, the thin electrode produced stable magnetic (H) fields while electric (E) fields increased with frequency. In contrast, the thick electrode demonstrated the inverse trend, emphasizing how electrode geometry can be used to modulate EM field output, potentially allowing for treatment personalization. Our RMS analysis provided additional insights into plasma electron dynamics. With a vertical PDT orientation at 14.5 kHz and 6V, the electron density peaked at 2.9×10^{11} electrons/m³. Whereas under the same frequency and voltage but with horizontal orientation, the peak density was slightly lower at 2.6×10^{11} electrons/m³ (Fig. 4). These measurements highlight how physical placement of the PDT influences plasma characteristics highlighting orientation as a critical factor for optimizing therapeutic delivery.

Moreover, harmonic estimation using near-field probes detected the presence of frequency components beyond the driving signal, including MHz and GHz harmonics (Figs. 5 and 6). These high-frequency emissions are generated by electron oscillations and density fluctuations within the plasma, suggesting that EM radiation from the PDT can exert

multi-scale biological effects, from organelle disruption to potential interference with DNA repair pathways, similar to TTF [54,55]. In this context, it is important to note that PDT therapy operates through a closed system that generates controlled EM fields and reactive species, offering a primarily physical treatment modality. In contrast, CAP jets and DBDs deliver ROS directly to biological targets, with CAP jets showing tumor inhibition [35,56] and DBDs inducing apoptosis with brief exposures [57]. TTFields, meanwhile, employ alternating electric fields (100–300 kHz) to disrupt mitosis and have demonstrated clinical efficacy in glioblastoma [26]. While PDT offers precise EM control and minimal thermal effects within a reproducible system, its application remains limited to in vitro studies. CAP and DBD therapies deliver direct ROS effects but depend on gas flow and exposure conditions, whereas TTFields are non-invasive and clinically validated but act mainly via antimitotic rather than oxidative mechanisms.

To capture EM field characteristics with precision, a three-axis sensor was placed directly on the PDT surface, ensuring no gap between sensor and tube. Each configuration was measured ten times to ensure accuracy and reproducibility. The electric field (E) was measured in volts per meter (V/m) and the magnetic field (H) in microtesla (μ T), allowing us to correlate field strength with plasma behavior and cellular effects (Figs. 7 and 8). To relate the physical diagnostics to biological outcomes, it is important to note that while EM emissions at ~16–17 GHz were measured (Fig. 4B) and power density at a distance of 10 cm from the PDT (Fig. 8), the in vitro experiments were performed with culture plates placed directly on top of the device (0 cm distance). At this

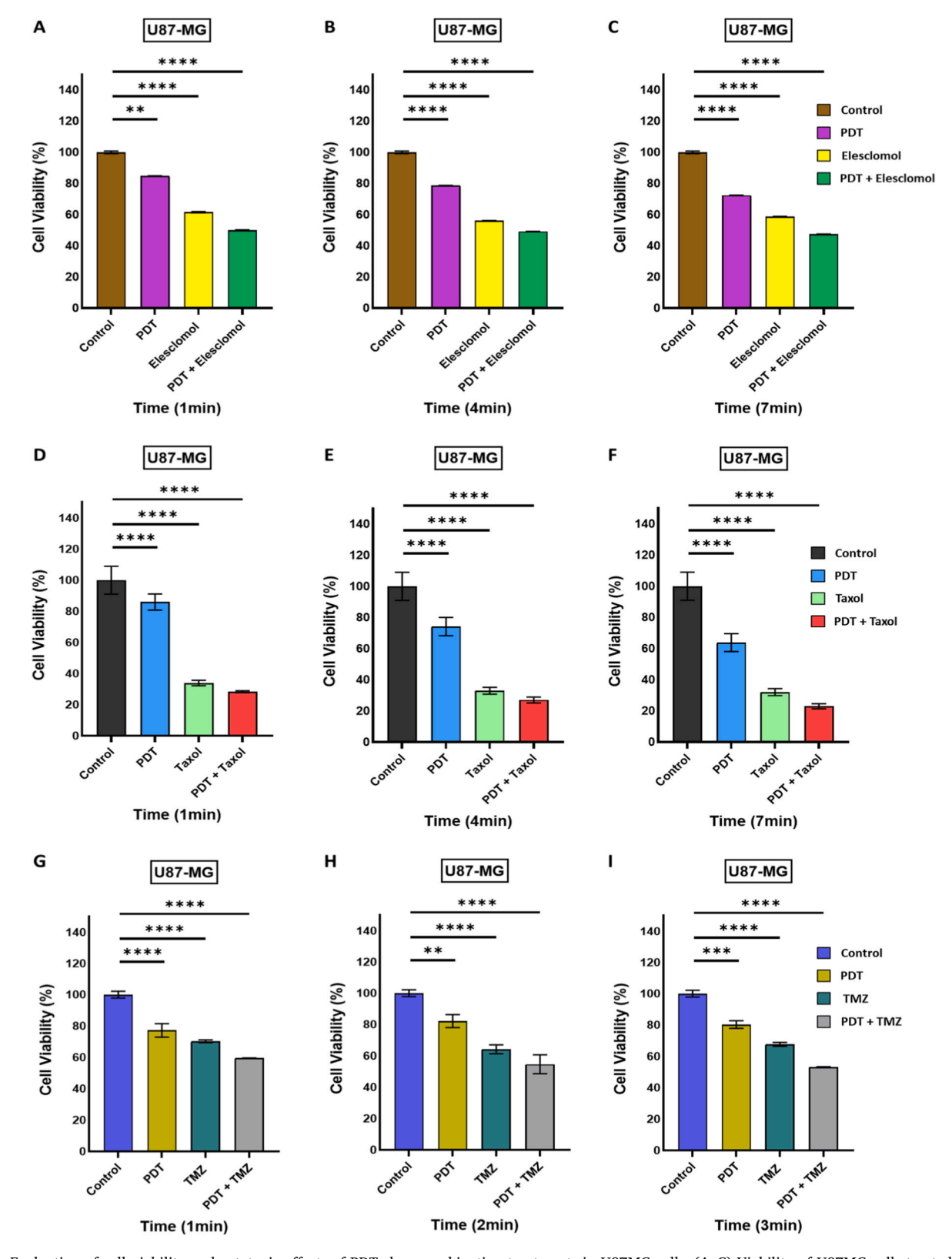


Fig. 10. Evaluation of cell viability and cytotoxic effects of PDT–drug combination treatments in U87MG cells. (A–C) Viability of U87MG cells treated with Eleschomol (STA-4783), (D–F) Taxol (Paclitaxel), and (G–I) Temozolomide (TMZ) in combination with PDT exposure for 1, 4, and 7 min (or 1, 2, and 3 min for TMZ). Each treatment set included four conditions: Control, PDT alone, Drug alone, and PDT + Drug. Data are presented as mean \pm SEM (n = 16 replicates per condition). Statistical significance was determined using two-way ANOVA followed by Tukey's multiple comparisons test (*p < 0.05, **p < 0.01, ***p < 0.001, ****p < 0.0001, ns = not significant).

proximity, cells are exposed to the full spectrum of plasma-generated EM fields and RONS which are responsible for the observed cytotoxic effects, and the treatments were optimized to achieve maximum effect. Therefore, EM emissions were mapped at distances up to 10 cm to characterize the field distribution and intensity. The spectroscopy and EM measurements provide a quantitative characterization of the device output, ensuring reproducibility and offering insight into the intensity and composition of the plasma environment experienced by the cells. This connection between the physical diagnostics and the in vitro setup helps interpret the biological responses and supports the translational relevance of the device for future preclinical or in vivo applications.

Biologically, combining PDT with chemotherapeutics such as Eleschomol, Taxol, or TMZ [33–36], resulted in enhanced anti-tumor effects in vitro (Figs. 9 and 10). PDT-generated EM and ROS damages mitochondrial and cellular structures, while the drugs induce ROS, cause microtubule depolymerization, cell cycle arrest, DNA alkylation and apoptosis. Their combined use is amplified cytotoxicity, likely by sensitizing tumor cells to chemotherapy through oxidative priming. Furthermore, the EM waves and harmonics produced during PDT exposure may help overcome TMZ resistance by perturbing DNA repair processes and chromatin dynamics [55].

Looking ahead, the potential for multi-discharge tube integration is especially promising. A modular PDT array can spatially modulate EM field intensity and composition, enabling customized treatment for heterogeneous tumors like GBM. Different tubes can be tuned to emit distinct field profiles, frequencies, and reactive species compositions. Coupled with real-time OES and EM field feedback, this system could dynamically adapt to tumor size, location, and molecular phenotype advancing toward precision plasma oncology and clinical translational medicine. This study demonstrates the transformative potential of tunable PDT technology to revolutionize cancer therapy by addressing the critical limitations of current treatment modalities. The ability to modulate EM field properties through electrode geometry, frequency adjustment, and orientation represents a paradigm shift from one-sizefits-all approaches to precision plasma oncology. The dual mechanism of action, combining direct cellular damage through RONS with EM field effects that can disrupt DNA repair pathways, offers a synergistic approach that could overcome treatment resistance mechanisms prevalent in aggressive cancers like glioblastoma. Most significantly, the prospect of multi-discharge tube integration opens possibilities for spatially customized treatment delivery, where different plasma configurations could be simultaneously applied to address tumor heterogeneity within a single patient. This personalized approach, guided by real-time optical emission spectroscopy and EM field monitoring, could enable dynamic treatment adaptation based on tumor response, location, and molecular characteristics. By combining the cytotoxic effects of PDT-generated species and EMF with the potential to enhance chemotherapy sensitivity and overcome drug resistance, this technology positions PDT as a versatile, non-invasive platform that could be integrated into existing oncological workflows while advancing toward truly personalized cancer treatment strategies. The demonstrated effects when combined with chemotherapeutics like Elesclomol, Taxol, and TMZ suggest broad applicability beyond glioblastoma, with potential for enhancing treatment efficacy across diverse cancer types through oxidative priming and electromagnetic sensitization of tumor cells to conventional drugs. While our previous in vivo studies have demonstrated that CAP jets can penetrate the skull and suppress intracranial tumor growth [36], the present in vitro study does not directly assess BBB permeability. The PDT system investigated here generates low-frequency EM waves and RONS, both of which may influence cellular transport and signaling; however, attributing any facilitation of drug delivery across the BBB to PDT remains speculative at this stage. Previous studies have shown that EM fields in defined frequency ranges can transiently alter BBB integrity in vivo [58-61], providing a conceptual basis for future investigation. Building upon our prior animal work and preliminary data [29], we are currently conducting in vivo

studies to directly evaluate whether PDT exposure modulates BBB permeability. In conclusion, this study affirms the versatility of the PDT system as a promising platform for non-invasive, multi-modal cancer treatment. Through a careful combination of physical tuning, harmonic control, spectral analysis, and orientation-based plasma optimization, PDT offers a new paradigm in adaptive cancer therapy. Future efforts will include in vivo validation, regulatory development, and clinical integration of this technology into standard neuro-oncology workflows.

5. Conclusion

This study highlights the transformative potential of the PDT system as a non-invasive and adaptable therapeutic platform for cancer treatment. In this study, we conducted a comprehensive physical and biological characterization of the PDT system for glioblastoma (GBM) treatment. Our results demonstrate that electrode geometry, placement, and discharge orientation critically modulate EM field strength and distribution, which correlates with observed variations in cell viability across A172, T98G, and U87MG, lines. Adjusting and fine-tuning these parameters enabled reproducible control over EM emissions and plasma uniformity, offering practical guidance for PDT device optimization. Furthermore, OES confirmed the presence of RONS that contribute to cytotoxic effects, while near-field probe and RMS diagnostics validated EM field characteristics and electron density, linking physical plasma properties with biological outcomes. Therapeutically, PDT demonstrated potent cytotoxic effects in glioblastoma cells, both as a standalone treatment and in combination with agents such as Elesclomol, Taxol, and TMZ. The observed synergy suggests that PDT-induced EM fields and plasma-generated species can sensitize tumor cells and potentially enhance drug efficacy. However, the implications for BBB permeability and in vivo translation require further experimental validation. These findings highlight the importance of integrating physical diagnostics with biological evaluation to understand plasma cell interactions and optimize PDT design. Overall, this work highlights the importance of tailoring electrode configuration, discharge parameters, and physical diagnostics to refine PDT design and therapeutic reproducibility. While the findings establish PDT as a promising non-invasive platform in plasma oncology, future studies will focus on molecular validation, in vivo optimization and modeling, therapeutic potential, and clinical translation to fully realize its potential in oncological therapy.

CRediT authorship contribution statement

Vikas Soni: Writing – review & editing, Writing – original draft, Visualization, Validation, Software, Methodology, Investigation, Formal analysis, Data curation, Conceptualization. Li Lin: Writing – review & editing, Validation, Software, Methodology, Formal analysis, Data curation. Anmol Taploo: Writing – review & editing, Validation, Software, Methodology, Formal analysis, Conceptualization. Jonathan H. Sherman: Writing – review & editing, Validation, Supervision, Resources, Project administration, Funding acquisition, Conceptualization. Michael Keidar: Writing – review & editing, Validation, Supervision, Resources, Project administration, Methodology, Investigation, Funding acquisition, Conceptualization.

Research resource identifiers (RRIDs)

The human glioblastoma cell lines A172 (RRID: CVCL_0131), T98G (RRID: CVCL_0556), and U87MG (RRID: CVCL_0022), were obtained from ATCC on June 20, 2019. These cell lines were authenticated by ATCC (American Type Culture Collection), which performs short tandem repeat (STR) profiling and mycoplasma testing as part of their standard quality control procedures prior to distribution. All three lines were confirmed to be mycoplasma-free by ATCC at the time of shipment. No additional in-lab authentication or mycoplasma testing was

performed by our team.

Ethics approval and consent to participate

This study did not involve human participants, human data, or animal subjects. As such, ethical approval and informed consent were not required. All experimental procedures were conducted exclusively on cell cultures and complied with institutional biosafety and research integrity guidelines applicable to in vitro studies.

Consent for publication

This manuscript does not contain any data from individual people, including identifiable details, images, or videos. As such, consent for publication is not applicable. All authors have thoroughly reviewed and approved the manuscript, and they collectively consent to its submission for consideration. We declare no conflicts of interest related to this work.

Statement of significance

We present a novel non-invasive Plasma Discharge Tube (PDT) for cancer treatment, incorporating a 3D-printed biocompatible support frame that enables precise electrode alignment and stable plasma generation. Unlike conventional plasma devices, our approach allows precise control over plasma exposure while maintaining compatibility with biological systems. This work is significant because it bridges materials physics and biomedicine, demonstrating potential applications in tumor treatment through localized plasma-mediated effects. The combination of a tunable, structurally robust material with plasma technology offers a versatile platform for biointerface studies, tissue engineering, and cancer therapy research. Our findings are expected to interest readers across biomaterials, biomedical engineering, and translational oncology.

Funding information

This work was supported by the National Science Foundation, Grant No. 1747760.

Declaration of competing interest

The authors declare that they have no known competing financial interests or personal relationships that could have appeared to influence the work reported in this paper.

Appendix A. Supplementary data

Supplementary data to this article can be found online at https://doi.org/10.1016/j.mtadv.2025.100660.

Data availability

The datasets generated and analyzed during the current study are available from the corresponding author on reasonable request. Raw data supporting the conclusions of this article are included within the article. Additional data that supports the findings of this study are available upon request from the corresponding author, subject to institutional review and approval.

References

- M. Laroussi, T. Akan, Arc-Free atmospheric pressure cold plasma jets: a review, Plasma Process. Polym. 4 (2007) 777–788, https://doi.org/10.1002/ ppap.200700066.
- [2] M. Keidar, A prospectus on innovations in the plasma treatment of cancer, Phys. Plasmas 25 (2018) 083504, https://doi.org/10.1063/1.5034355.

- [3] C. Tendero, C. Tixier, P. Tristant, J. Desmaison, P. Leprince, Atmospheric pressure plasmas: a review, Spectrochimica Acta. Part B, Atomic Spectroscopy 61 (2006), https://doi.org/10.1016/j.sab.2005.10.003.
- [4] X. Lu, K. Ostrikov, Ken, Guided ionization waves: the physics of repeatability, Appl. Phys. Rev. 5 (2018) 031102, https://doi.org/10.1063/1.5031445.
- [5] X. Lu, G.V. Naidis, M. Laroussi, S. Reuter, D.B. Graves, K. Ostrikov, Reactive species in non-equilibrium atmospheric-pressure plasmas: generation, transport, and biological effects, Phys. Rep. 630 (2016) 1–84, https://doi.org/10.1016/j. physrep.2016.03.003.
- [6] D.B. Graves, The emerging role of reactive oxygen and nitrogen species in redox biology and some implications for plasma applications to medicine and biology, J. Phys. D Appl. Phys. 45 (2012) 263001, https://doi.org/10.1088/0022-3727/45/ 26/763001
- [7] M. Keidar, Plasma for cancer treatment, Plasma Sources Sci. Technol. 24 (2015) 033001, https://doi.org/10.1088/0963-0252/24/3/033001.
- [8] G. Bauer, D.B. Graves, Mechanisms of selective antitumor action of cold atmospheric plasma-derived reactive oxygen and nitrogen species, Plasma Process. Polym. 13 (2016), https://doi.org/10.1002/ppap.201600089.
- [9] S. Bekeschus, et al., A comparison of floating-electrode DBD and kINPen jet: plasma parameters to achieve similar growth reduction in Colon cancer cells under standardized conditions, Plasma Chem. Plasma Process. 38 (2018) 1–12.
- [10] M. Xaubet, et al., Comparative study of the reactive species in the effluent of two different plasma jet devices operated with air as working gas, J. Phys. D Appl. Phys. 58 (2025) 365201.
- [11] M. Keidar, D. Yan, I.I. Beilis, B. Trink, J.H. Sherman, Plasmas for treating cancer: opportunities for adaptive and self-adaptive approaches, Trends Biotechnol. 36 (2018) 586–593, https://doi.org/10.1016/j.tibtech.2017.06.013.
- [12] D.B. Graves, Mechanisms of plasma medicine: coupling plasma physics, biochemistry, and biology, IEEE Transactions on Radiation and Plasma Medical Sciences 1 (2017) 281–292, https://doi.org/10.1109/TRPMS.2017.2710880.
- [13] E. Gjika, et al., Combination therapy of cold atmospheric plasma (CAP) with temozolomide in the treatment of U87MG glioblastoma cells, Sci. Rep. 10 (2020) 16495.
- [14] E. Gjika, et al., Adaptation of operational parameters of cold atmospheric plasma for in vitro treatment of cancer cells, ACS Appl. Mater. Interfaces 10 (2018) 9269–9279.
- [15] W. Murphy, A. Horkowitz, V. Soni, C. Walkiewicz-Yvon, M. Keidar, Dual-Plasma discharge tube for synergistic glioblastoma treatment, Cancers 17 (2025) 2036.
- [16] J. Sun, et al., Effects of extremely low frequency electromagnetic fields on the tumor cell inhibition and the possible mechanism, Sci. Rep. 13 (2023) 6989.
- [17] M. Huang, et al., Is extremely low frequency pulsed electromagnetic fields applicable to gliomas? A literature review of the underlying mechanisms and application of extremely low frequency pulsed electromagnetic fields, Cancer Med. 12 (2022) 2187–2198, https://doi.org/10.1002/cam4.5112.
- [18] Y. Liu, et al., Low-frequency magnetic field therapy for glioblastoma: current advances, mechanisms, challenges and future perspectives, J. Adv. Res. 69 (2025) 531–543.
- [19] H. Wang, X. Zhang, Magnetic fields and reactive oxygen species, Int. J. Mol. Sci. 18 (2017) 2175.
- [20] S. Hambarde, J.M. Manalo, D.S. Baskin, M.A. Sharpe, S.A. Helekar, Spinning magnetic field patterns that cause oncolysis by oxidative stress in glioma cells, Sci. Rep. 13 (2023) 19264.
- [21] D.B. Zolotukhin, A. Horkowitz, M. Keidar, Electromagnetic nature of distant interaction of the atmospheric pressure helium plasma discharge tube with glioblastoma cancer cells, ACS Appl. Mater. Interfaces 16 (2024) 13597–13610.
- [22] L. Lin, M. Keidar, A map of control for cold atmospheric plasma jets: from physical mechanisms to optimizations, Appl. Phys. Rev. 8 (2021) 011306, https://doi.org/ 10.1063/5.0022534
- [23] X.-W. Xiang, H.-T. Liu, X.-N. Tao, Y.-L. Zeng, J. Liu, C. Wang, S.-X. Yu, H. Zhao, Y.-J. Liu, K.-F. Liu, Glioblastoma behavior study under different frequency electromagnetic field, iScience 26 (2023) 108575, https://doi.org/10.1016/j.isri.2023.108575.
- [24] X. Guo, et al., Tumor-treating fields in glioblastomas: past, present, and future, Cancers (Basel) 14 (2022) 3669.
- [25] R. Stupp, et al., Effect of tumor-treating fields plus maintenance temozolomide vs maintenance temozolomide alone on survival in patients with glioblastoma: a randomized clinical trial, JAMA 318 (2017) 2306–2316.
- [26] S. Khagi, et al., Recent advances in Tumor treating Fields (TTFields) therapy for glioblastoma, Oncologist 30 (2025) oyae227.
- [27] Y. Liu, Q. Tang, Q. Tao, H. Dong, Z. Shi, L. Zhou, Low-frequency magnetic field therapy for glioblastoma: current advances, mechanisms, challenges and future perspectives, J. Adv. Res. (2024), https://doi.org/10.1016/j.jare.2024.03.024.
- [28] O. Rominiyi, A. Vanderlinden, S.J. Clenton, C. Bridgewater, Y. Al-Tamimi, S. J. Collis, Tumour treating fields therapy for glioblastoma: current advances and future directions, Br. J. Cancer 124 (2021) 697–709.
- [29] Xiaoliang Yao, Li Lin, Vikas Soni, Eda Gjika, Jonathan H. Sherman, Dayun Yan, Michael Keidar, Sensitization of glioblastoma cells to temozolomide by a helium gas discharge tube, Phys. Plasmas 27 (11) (2020) 114502, https://doi.org/ 10.1063/5.0017913.
- [30] X. Cheng, et al., Enhancing cold atmospheric plasma treatment of cancer cells by static magnetic field, Bioelectromagnetics 38 (2017) 53–62.
- [31] L. Lin, Y. Lyu, B. Trink, J. Canady, M. Keidar, Cold atmospheric helium plasma jet in humid air environment, J. Appl. Phys. 125 (2019) 153301, https://doi.org/ 10.1063/1.5086177
- [32] L. Lin, M. Keidar, Cold atmospheric plasma jet in an axial DC electric field, Phys. Plasmas 23 (2016) 083529, https://doi.org/10.1063/1.4961924.

- [33] V. Soni, M. Adhikari, H. Simonyan, L. Lin, J.H. Sherman, C.N. Young, M. Keidar, In vitro and in vivo enhancement of temozolomide effect in human glioblastoma by non-invasive application of cold atmospheric plasma, Cancers 13 (2021) 4485, https://doi.org/10.3390/cancers13174485.
- [34] V. Soni, M. Adhikari, L. Lin, J.H. Sherman, M. Keidar, Theranostic potential of adaptive cold atmospheric plasma with temozolomide to checkmate glioblastoma: an In vitro study, Cancers (Basel) 14 (2022) 3116, https://doi.org/10.3390/ cancers14133116.
- [35] V. Soni, T. Dawson, L. Lin, K. Crandall, J. Sherman, M. Keidar, High-Throughput RNA-Seq and In-Silico analysis of glioblastoma cells treated with cold atmospheric plasma and temozolomide, Preprint at, https://doi.org/10.21203/rs.3.rs-4 569010/v2, 2024.
- [36] V. Soni, Application of cold atmospheric plasma in the treatment of cancer, viruses, and bacteria. Proquest Dissertations and Theses, The George Washington University, United States District of Columbia, 2024. https://www.proquest.com/pqdtlocal1006561/docview/3098034866/277CE826120444DDPQ/2?accountid=11243&sourcetype=Dissertations%20&%20Theses.
- [37] I.E. Kieft, J.L.V. Broers, V. Caubet-Hilloutou, D.W. Slaaf, F.C.S. Ramaekers, E. Stoffels, Plasma-induced effects on mammalian cells, New J. Phys. 6 (2004) 41.
- [38] M. Gallardo-Villagrán, L. Paulus, D.Y. Leger, B. Therrien, B. Liagre, Dimethyl sulfoxide: a bio-friendly or bio-hazard chemical? The effect of DMSO in human fibroblast-like synoviocytes, Molecules 27 (2022) 4472.
- [39] C. Zhang, et al., Effects of dimethyl sulfoxide on the morphology and viability of primary cultured neurons and astrocytes, Brain Res. Bull. 128 (2017) 34–39.
- [40] G. Da Violante, et al., Evaluation of the cytotoxicity effect of dimethyl sulfoxide (DMSO) on Caco2/TC7 colon tumor cell cultures, Biol. Pharm. Bull. 25 (2002) 1600–1603
- [41] K.F. Chu, D.B. Dupuy, Thermal ablation of tumors: biological mechanisms and advances in therapy, Nat. Rev. Cancer 14 (3) (2014) 199–208.
- [42] Amazon.com: foriot 9-12V radio frequency wideband amplifier low noise amplifier LNA 0.1-2000mhz gain 32db: electronics. (n.d.). https://www.amazon.com/FO RIOT-Frequency-Wideband-Amplifier-0-1-2000MHz/dp/B0CFLB7QLF.
- [43] EMF Detector, MESTEK EMF01 electromagnetic radiation Tester(5-3500MHZ). https://www.mestek-tools.com/en/productdetail.aspx?detailid=167.
- [44] H. Ohgaki, P. Kleihues, The definition of primary and secondary glioblastoma, Clin. Cancer Res. 19 (2013) 764–772, https://doi.org/10.1158/1078-0432.CCR-12-2003
- [45] R. Stupp, E.T. Wong, A.A. Kanner, D. Steinberg, H. Engelhard, V. Heidecke, E. D. Kirson, S. Taillibert, F. Liebermann, V. Dbalý, et al., NovoTTF-100A versus physician's choice chemotherapy in recurrent glioblastoma: a randomised phase III trial of a novel treatment modality, Eur. J. Cancer 48 (2012) 2192–2202, https://doi.org/10.1016/j.ejca.2012.04.011.

- [46] G. Fridman, et al., Applied plasma medicine, Plasma Process. Polym. 5 (2008) 503–533.
- [47] V. Novickij, N. Rembiałkowska, W. Szlasa, J. Kulbacka, Does the shape of the electric pulse matter in electroporation? Front. Oncol. 12 (2022).
- [48] A. Privat-Maldonado, et al., ROS from physical plasmas: Redox chemistry for biomedical therapy, Oxid. Med. Cell. Longev. 2019 (2019) 9062098.
- [49] H.J. Ahn, et al., Targeting cancer cells with reactive oxygen and nitrogen species generated by atmospheric-pressure air plasma, PLoS One 9 (2014) e86173.
- [50] B. Perillo, et al., ROS in cancer therapy: the bright side of the moon, Exp. Mol. Med. 52 (2020) 192–203.
- [51] H. Nakamura, K. Takada, Reactive oxygen species in cancer: current findings and future directions, Cancer Sci. 112 (2021) 3945–3952.
- [52] C.A. Juan, J.M. Pérez de la Lastra, F.J. Plou, E. Pérez-Lebeña, The chemistry of reactive Oxygen Species (ROS) revisited: outlining their role in biological macromolecules (DNA, lipids and proteins) and induced pathologies, Int. J. Mol. Sci. 22 (2021) 4642.
- [53] R. Huang, et al., Dual role of reactive oxygen species and their application in cancer therapy, J. Cancer 12 (2021) 5543–5561.
- [54] M. Salzberg, E. Kirson, Y. Palti, C. Rochlitz, A pilot study with very low-intensity, intermediate-frequency electric fields in patients with locally advanced and/or metastatic solid tumors, Onkologie 31 (2008) 362–365, https://doi.org/10.1159/00012712
- [55] K. Yoshimoto, M. Mizoguchi, N. Hata, H. Murata, R. Hatae, T. Amano, A. Nakamizo, T. Sasaki, Complex DNA repair pathways as possible therapeutic targets to overcome temozolomide resistance in glioblastoma, Front. Oncol. 2 (2012) 186, https://doi.org/10.3389/fonc.2012.00186.
- [56] T. Fang, Z. Chen, G. Chen, Advances in cold atmospheric plasma therapy for cancer, Bioact. Mater. 53 (2025) 433–458.
- [57] S.B. Karki, E. Yildirim-Ayan, K.M. Eisenmann, H. Ayan, Miniature dielectric barrier discharge nonthermal plasma induces apoptosis in lung cancer cells and inhibits cell migration, BioMed Res. Int. 2017 (2017) 8058307.
- [58] B.R.R. Persson, L.G. Salford, A. Brun, Blood-brain barrier permeability in rats exposed to electromagnetic fields used in wireless communication, Wirel. Netw. 3 (1997) 455–461.
- [59] L.G. Salford, A. Brun, K. Sturesson, J.L. Eberhardt, B.R.R. Persson, Permeability of the blood-brain barrier induced by 915 MHz electromagnetic radiation, continuous wave and modulated at 8, 16, 50, and 200 Hz, Microsc. Res. Tech. 27 (1994) 535–542
- [60] P. Gao, et al., Effect of ultra-wide-band electromagnetic pulses on blood-brain barrier permeability in rats, Mol. Med. Rep. 22 (2020) 2775–2782.
- [61] R. Stam, Electromagnetic fields and the blood-brain barrier, Brain Res. Rev. 65 (2010) 80–97.